Plant Physiology Preview. Published on April 25, 2012, as DOI:10.1104/pp.111.192575

Plasma membrane calcium ATPases are important components of receptor-mediated signalling in plant immune responses and development

Nicolas Frei dit Frey[1,7], Malick Mbengue[2], Mark Kwaaitaal[1], Lisette Nitsch[3], Denise Altenbach[1], Heidrun Häweker[1,2], Rosa Lozano-Duran[2], Maria Fransiska Njo[4,5], Tom Beeckman[4,5], Bruno Huettel[1], Jan Willem Borst[3], Ralph Panstruga[1,6], and Silke Robatzek[1,2,#]

[1]Max-Planck-Institute for Plant Breeding Research, Carl-von-Linné-Weg 10, 50829 Köln, Germany

[2]The Sainsbury Laboratory, Norwich Research Park, Norwich, NR4 7UH, UK

[3]Wageningen University, Laboratory of Biochemistry, Microspectroscopy Centre, Dreijenlaan 3, 6703HA, Wageningen, The Netherlands

[4]Department of Plant Systems Biology, Flanders Institute for Biotechnology, 9052 Ghent, Belgium

[5]Department Plant Biotechnology and Bioinformatics, Ghent University, 9052 Ghent, Belgium

[6]RWTH Aachen University, Institute for Biology I, Unit of Plant Molecular Cell Biology, 52056 Aachen, Germany

[7]Present address: INRA-CNRS, UMR1165, Unité de Recherche en Génomique Végétale, 2 rue Gaston Crémieux, F-91057 Evry, France

[#]Corresponding author: Silke Robatzek

Short title: ACA8/10-mediated flg22 responses and immunity

Keywords: PAMP, flg22, receptor kinase, calcium signalling, ACA8, ACA10

Word count: abstract (246); total text (57,062 characters with spaces including figure legends); references (68)

Abstract

Plasma membrane-resident receptor kinases (RKs) initiate signalling pathways important for plant immunity and development. In *Arabidopsis thaliana*, the receptor for the elicitor-active peptide epitope of bacterial flagellin, flg22, is encoded by FLS2, which promotes plant immunity. Despite its relevance, the molecular components regulating the FLS2-mediated signalling remain largely unknown. We show that the plasma membrane calcium (Ca^{2+}) ATPase ACA8 forms a complex with FLS2 *in planta*. ACA8 and its closest homologue ACA10 are required for limiting the growth of virulent bacteria. One of the earliest flg22 responses is the transient increase of cytosolic Ca^{2+} ions, which is crucial for many of the well-described downstream responses, e.g. generation of reactive oxygen species (ROS) and the transcriptional activation of defence-associated genes. Mutant *aca8 aca10* plants show decreased flg22-induced Ca^{2+} and ROS bursts, and exhibit altered transcriptional reprogramming. In particular, mitogen-activated protein kinase (MAPK)-dependent flg22-induced gene expression is elevated, while calcium-dependent protein kinase (CDPK)-dependent flg22-induced gene expression is reduced. These results demonstrate that the fine regulation of Ca^{2+} fluxes across the plasma membrane is critical for the coordination of the downstream MAMP responses and suggest a mechanistic link between the FLS2 receptor complex and signalling kinases via the secondary messenger Ca^{2+}. ACA8 also interacts with other RKs such as BRI1 and CLV1 known to regulate plant development, and both *aca8* and *aca10* mutants show morphological phenotypes, suggesting additional roles for ACA8 and ACA10 in developmental processes. Thus, Ca^{2+} ATPases appear to represent general regulatory components of RK-mediated signalling pathways.

Introduction

Receptor kinases (RKs) constitute a large gene family in plants with more than 600 members in *A. thaliana*, and are key to ligand-mediated signalling pathways in plant immunity and development (Shiu and Bleecker, 2001). Only a handful of RKs have been studied in detail and matched with their cognate ligand, of which FLAGELLIN SENSING 2 (FLS2), EF-TU RECEPTOR (EFR), and XA21 encode leucine-rich repeat (LRR)-RKs conferring perception of microbe-associated molecular patterns (MAMPs) from bacteria in Arabidopsis and rice (*Oryza sativa*), respectively, (Zipfel, 2009). Perception of the fungal MAMP chitin involves the LysM-RK CHITIN ELICITOR RECEPTOR KINASE 1 (CERK1). FLS2 detects a conserved peptide at the N-terminus of bacterial flagellin (flg22) and forms an inducible complex with BRI1-ASSOCIATED KINASE 1/SOMATIC EMBRYO RECEPTOR KINASE 3 (BAK1/SERK3), an LRR-RK initially identified as co-receptor of BRASSINOSTEROID INSENSITIVE 1 (BRI1) regulating brassinosteroid signalling and now reported to also act in various immune pathways and cell death control (Chinchilla et al., 2009; Postel et al., 2010; Schulze et al., 2010; Fradin et al., 2011; Schwessinger et al., 2011). The manifold phenotypes of *bak1/serk3* mutant plants suggest that BAK1/SERK3 can potentially interact with multiple RKs to regulate a number of different signalling pathways. This offers the possibility for molecular crosstalk between different RK-mediated signalling pathways, as recently demonstrated for brassinosteroid signalling negatively impacting flg22 responses (Albrecht et al., 2012; Belkhadir et al., 2012). At the molecular level, BAK1/SERK3 was shown to transphosphorylate BRI1 and EFR (Wang et al., 2008; Chen et al., 2010; Schwessinger et al., 2011). Moreover, BRI1, FLS2 and EFR can associate with other members of the SERK family revealing some levels of functional redundancy (Albrecht et al., 2008; Roux et al., 2011).

Interaction between the ligand-binding RKs BRI1, FLS2, EFR and BAK1/SERK3, respectively, is required for proper downstream responses (Chinchilla et al., 2007). One of the earliest responses stimulated by MAMPs are changes in ion fluxes across the plasma membrane, which result in an increased level of calcium ions (Ca^{2+}) in the cytosol (Blume et al., 2000; Wendehenne et al., 2002; Jeworutzki et al., 2010). Ca^{2+} acts as an important second messenger for a multitude of biotic and abiotic stimuli, whereas different signals trigger unique Ca^{2+} signatures (Dodd et al., 2010; Kudla et al., 2010). MAMPs typically induce a transient Ca^{2+} burst, resulting in a rapid (within seconds) increase of free cytosolic Ca^{2+}, which subsequently (within minutes) declines to steady-state Ca^{2+} levels (Blume et al., 2000;

Ranf et al., 2008). The Ca^{2+} burst occurs upstream of many MAMP-elicited responses including the rapid production of reactive oxygen species (ROS), activation of signalling kinases, as well as changes in gene expression (Blume et al., 2000; Boller and Felix, 2009; Ranf et al., 2011; Segonzac et al., 2011). However, genetic studies and identification of the underlying molecular components of the MAMP-induced Ca^{2+} burst are largely missing (Ranf et al., 2008; Boller and Felix, 2009). In general, cytosolic Ca^{2+} levels are regulated by plasma membrane- and endomembrane-bound Ca^{2+} channels that mediate influx of Ca^{2+} and efflux transporters that re-establish Ca^{2+} homeostasis. A number of ion channels have been identified, some of which have roles in plant immunity such as DEFENSE NO DEATH 1 (DND1) (Clough et al., 2000; Lamotte et al., 2004; Kudla et al., 2010). Recently, ionotropic glutamate receptor-like proteins (iGLRs) were shown to regulate Ca^{2+} influx at the plasma membrane and were also implicated in MAMP-induced responses (Cho et al., 2009; Kwaaitaal et al., 2011; Michard et al., 2011; Vatsa et al., 2011), and an ER-localized P2A-type Ca^{2+} ATPase was described to contribute to pathogen-induced cell death and to alter the MAMP-triggered Ca^{2+} burst (Zhu et al., 2010). The relevance of Ca^{2+} influx in MAMP-elicited responses is underlined by polysaccharides secreted from bacterial pathogens to chelate Ca^{2+} in the apoplastic space (Aslam et al., 2008).

Here, we report that the plasma membrane resident P2B-type Ca^{2+} ATPase ACA8 interacts with FLS2 *in planta*. Loss-of-function *aca8* plants, the mutant of its closest homologue *aca10*, and the *aca8 aca10* double mutant were more susceptible to bacterial infection. Analysing individual MAMP responses, *aca8 aca10* mutant plants displayed decreased flg22-triggered Ca^{2+} influx and ROS accumulation. Importantly, flg22-triggered gene expression downstream of MAPK signalling was increased, but reduced for gene expression downstream of CDPK signalling. This suggests that the MAMP-induced Ca^{2+} burst is required for proper transcriptional reprogramming upon elicitation. According to their function as Ca^{2+} pumps, ACA8 and ACA10 are hypothesized to regulate Ca^{2+} efflux during the flg22-elicited Ca^{2+} burst, which suggests a molecular link between the FLS2 receptor, Ca^{2+} signalling and flg22-triggered downstream responses. In addition, *aca8* and *aca8 aca10* mutant plants showed developmental phenotypes affecting inflorescence height as well as root length. Together with the finding that ACA8 also interacts with other RKs such as BRI1 and CLV1, these results suggest that plasma membrane Ca^{2+} ATPases function in multiple RK-mediated signalling pathways.

Results

ACA8 interacts with FLS2 and other RKs

In a proteomics approach, we previously isolated proteins co-localizing to FLS2 in plasma membrane microdomains (Keinath et al., 2010). To address whether some of these proteins can associate with FLS2, we focussed on Ca^{2+} ATPases, which have also been identified as differentially phosphorylated and transcriptionally induced in response to flg22 (Zipfel et al., 2004; Benschop et al., 2007). ACA8 and ACA10 belong to the family of type 2B auto-inhibited Ca^{2+} ATPases consisting of ten members in Arabidopsis (Figure S1A; (Boursiac and Harper, 2007). These Ca^{2+} ATPases comprise ten transmembrane spanning domains, harbour a calmodulin binding domain for auto-inhibition of the ATPase active site, and can localize to different membrane compartments (Boursiac and Harper, 2007). ACA8, ACA9 and ACA10 group into a distinct subfamily and accumulate at the plasma membrane (Bonza et al., 2000; Hwang et al., 2000; Lee et al., 2007). While ACA9 expression is restricted to pollen and thereby is critical for pollen tube development, ACA8 and ACA10 are expressed throughout the plant and have not yet assigned any specific function besides inflorescence growth (Schiott et al., 2004).

We transiently expressed FLS2 and ACA8 fused to the N- and C-terminal halves of YFP, respectively, in *Nicotiana benthamiana* and examined possible protein-protein interactions by confocal microscopy in a so-called bimolecular fluorescence complementation (BiFC) assay (Bracha-Drori et al., 2004). In this assay, we observed reconstitution of the YFP molecule by detection of fluorescence when expressing FLS2 fused to both of the YFP halves indicative of FLS2 homodimerization (Figure 1A). We also observed BiFC when FLS2 was co-expressed with ACA8. As BiFC assays are based on transient expression in a heterologous system, the tagged proteins can accumulate to high levels facilitating the reconstitution of a BiFC signal, and thus ACA12, BRI1 and CLV1 were included as controls. No YFP reconstitution could be detected upon co-expressing of FLS2 and ACA12, another plasma membrane resident Ca^{2+} ATPase. Notably, ACA8 showed a broader interaction pattern, because BiFC was also observed with other RKs such as BRI1 and CLV1, of which the latter is functioning in stem cell identity maintenance and is normally not expressed in leaf tissue (Waites and Simon, 2000). Similar to FLS2, both BRI1 and CLV1 formed homodimers in this assay, but unlike FLS2 they also interacted with ACA12 (Figure 1A). In all cases of BiFC, the YFP signal was recorded at the cell periphery suggesting complex formation at the plasma membrane.

To further overcome limitations of BiFC assays we performed Förster Resonance Energy Transfer (FRET) measurements on the basis of Fluorescence Lifetime Imaging Microscopy (FLIM) using respective FLS2 and ACA8 fusions to CFP or YFP. FRET can be detected using FLIM where reduction of the fluorescence lifetime of a donor-containing molecule occurs due to proximity of an acceptor-containing molecule, which is an indication of physical interaction. We examined FLS2-ACA8 association in protoplasts from soil-grown Arabidopsis plants. Under this condition we observed a significant reduction in fluorescence lifetime when FLS2-CFP and ACA8-YFP were co-expressed as compared to the fluorescence lifetime of ACA8-CFP alone (Figure 1B; Table S1). Similar results were obtained when we used FLS2-CFP and ACA8-YFP. This suggests that both proteins are in close proximity to each other, indicative of protein-protein interaction. Interaction of fluorophore-tagged FLS2 and ACA8 was detected at the plasma membrane, which is in line with the subcellular localization of the two proteins and substantiates our findings of BiFC in *N. benthamiana*. However, interaction of fluorophore-tagged FLS2 and ACA8 was not distributed uniformly across the plasma membrane, but seen as patchy areas with strongly reduced fluorescence lifetimes (Figure 1B), which indicates the presence of FLS2-ACA8 complexes were restricted to subdomains within the plasma membrane. This observation is in agreement with the notion that FLS2 and ACA8 can localize to flg22-induced plasma membrane microdomains (Keinath et al., 2010). Despite numerous attempts we failed to clone a full-length *ACA10* cDNA, which precluded analysis of ACA10 by fluorophore-based interaction assays. Despite poor results by co-immunoprecipitation analysis, pull-down experiments of FLS2-GFP followed by mass-spectrometric analysis repeatedly revealed presence of ACA8 and ACA10 peptides, further corroborating the existence of FLS2-ACA8 and FLS2-ACA10 complexes *in planta* (Figure S2). Taken together, these results indicate that FLS2 forms a complex with ACA8 at the plasma membrane, and ACA8 can interact with multiple RKs, pointing at an important role in the regulation of RK-mediated signalling pathways.

ACA8 and ACA10 exhibit partial overlapping functions

To address ACA8 function, we isolated a T-DNA insertion line and a tilling mutant (both in Col-0 genetic background) in the *ACA8* gene (Fig. S1*B*). Genetic redundancy within members of the *ACA* family has been documented, and could be expected for members of the *ACA8*, *ACA9*, *ACA10* subgroup (Boursiac and Harper, 2007). Because *ACA9* expression was specific to pollen tubes, we focussed on *ACA10*, isolated a T-DNA insertion line in the *ACA10* gene, and generated *aca8 aca10* double knock-out lines (Figure S1C). In addition, we

crossed a *35S::ACA8-GFP* expressing transgenic line into the *aca8 aca10* double mutant. Single *aca8* mutants displayed no obvious developmental phenotypes (Figure 2). By contrast, *aca10* mutant plants were reduced in inflorescence height and displayed increased axillary stem formation, which was further enhanced in *aca8 aca10* plants (Figure 2A). This phenotype was also present in *aca10* plants crossed with the *aca8*^{Q70*} tilling mutant (Figure S3), and could be rescued by ectopic *ACA8-GFP* expression, demonstrating functional complementation by the GFP fusion protein (Figure 2A). Redundant functions of ACA8 and ACA10 in the regulation of inflorescence height were previously reported in Arabidopsis Wassilewskaja (Ws) background (George et al., 2008). Differences between the single mutants may result from an incomplete overlap of the *ACA8* and *ACA10* expression patterns. We did not observe any obvious mutant phenotype in rosette leaf development among the genotypes (Figure 2B), while *aca8 aca10* mutants showed significantly reduced root growth when cultivated *in vitro* (Figure 2C). Reduction in root growth was affecting primary root length and could be correlated with an early differentiation of stem cells compared to wild type plants (Figure S3).

Flg22-triggered early responses depend on ACA8 and ACA10 function

Ca^{2+} ATPases are responsible for extruding Ca^{2+} ions from the cytosol into endomembrane compartments or extracellularly into the apoplast (Bonza et al., 2004; Conn et al., 2011). ACA8 has been shown to mediate Ca^{2+} transport in yeast and is activated by binding of calmodulin (CaM) to its N-terminus (Bonza et al., 2000; Bonza et al., 2004; Mersmann et al., 2010). Based on the interaction of ACA8 with FLS2, we addressed whether ACA8 and ACA10 function in the flg22-triggered Ca^{2+} burst. All genotypes were therefore crossed to a transgenic line expressing the aequorin (Aeq) Ca^{2+} biosensor (Knight et al., 1991). We performed luminescence-based measurements of free cytosolic Ca^{2+} and revealed slightly elevated constitutive Ca^{2+} levels in *aca8 aca10 Aeq* plants (Figure S4). We then monitored the MAMP-induced Ca^{2+} burst over time. Mutant *aca8 Aeq* and *aca10 Aeq* plants responded like wild type upon flg22 treatment. By contrast, the flg22-triggered Ca^{2+} burst was strongly reduced in the *aca8 aca10 Aeq* lines and completely abolished in *fls2 Aeq* plants (Figure 3A; Figure S5). The overall pattern of the transient increase of Ca^{2+} remained similar between wild type and the *aca8 Aeq* and *aca10 Aeq* genotypes, but the maximal influx (peak) of the Ca^{2+} signature was affected in *aca8 aca10 Aeq* plants (Figure S5). The Ca^{2+} burst in response to chitin was slightly reduced in *aca8 aca10 Aeq* lines and for all other genotypes indistinguishable from wild type (Figure 3A). The lower peak in flg22-induced cytosolic Ca^{2+}

influx in the double mutant demonstrates that ACA8 and ACA10 both contribute to the flg22-elicited Ca^{2+} burst and indicates a role for these proteins in the regulation of FLS2-mediated early responses.

Production of ROS upon MAMP treatments is mediated by plasma membrane-resident NADPH oxidases, which depend on Ca^{2+} signalling for their function (Kobayashi et al., 2007; Mersmann et al., 2010). We examined the flg22-triggered oxidative burst and detected no significant differences between wild-type plants and the *aca8* and *aca10* single mutants, while the *aca8 aca10* double mutant displayed an overall decreased ROS production when treated with flg22 (Figure 3B). ROS production upon chitin treatment remained comparable to wild type in all tested mutants. The decrease in oxidative burst correlated with the reduced flg22-triggered Ca^{2+} signature in *aca8 aca10* plants, which is in agreement with Ca^{2+} operating upstream of ROS production. When monitoring these individual MAMP responses we observed genetic redundancy between *ACA8* and *ACA10* suggesting that both Ca^{2+} ATPases exert overlapping functions in these early and transient flg22 responses, which is in contrast to the unequal role of *ACA8* and *ACA10* in development. Western blot analysis revealed unaltered FLS2 protein accumulation in the *aca* mutants compared to wild type plants (Figure 3C). Therefore the observed reduction in flg22-triggered Ca^{2+} and ROS bursts is likely caused by loss-of-*ACA8* and -*ACA10* function rather than altered FLS2 levels.

ACA8 and ACA10 are required for proper flg22-induced transcriptional changes

For more detailed analysis of ACA8/ACA10 functions, we determined the transcriptional changes caused by *ACA8 ACA10* loss-of-function by microarray analysis. A total of 69 transcripts were identified as showing significantly elevated transcript levels and ten had significantly lower transcript abundance in the *aca8 aca10* double mutant compared to wild type seedlings (Table S2). We validated differential transcript accumulation of 19 out of 20 tested genes by quantitative RT-PCR analysis, of which 17 showed wild type-like expression in the *aca8 aca10*/*35S::ACA8-GFP* line, further substantiating functionality of the ACA8-GFP fusion protein (Table S2). Most remarkably, genes belonging to the GO categories "calcium ion binding" and "cation binding" were overrepresented among the genes that show higher transcript levels in the *aca8 aca10* double mutant (Table S2). The first category includes genes coding for CaM-like proteins such as CML35, CML36, CML41, CML45, CML46, CML47 (McCormack et al., 2005). Increased expression of *CaM*-like genes could be a compensatory mechanism to counteract the deficiency in extruding Ca^{2+} ions from the cytosol in *aca8 aca10* plants.

Only a small number of the *aca8 aca10* de-regulated genes were associated with plant defence (Table S2). One of them encodes ACD6, a regulator of SA-mediated disease resistance (Lu et al., 2003). Significantly reduced *ACD6* transcript levels in *aca8 aca10* plants may contribute to the enhanced susceptibility to *Pto*DC3000. To find out whether any of the other genes that exhibit differential transcript levels in *aca8 aca10* has a potential role in MAMP-triggered immunity, we searched publicly available transcriptome databases and identified 27 of the *aca8 aca10* up-regulated genes to be induced in response to MAMP treatments (Figure S6A). We then focussed on genes downstream of flg22 Ca^{2+} signalling (Boudsocq et al., 2010). There was only little overlap between the *aca8 aca10* de-regulated and CDPK-dependent genes (Figure S6C), which could be due to the different plant materials used for transcript profiling. We therefore studied flg22-induced expression of selected marker genes specifically downstream of the MAPK and/or CDPK cascade (Boudsocq et al., 2010). Flg22-induced expression of MAPK-regulated *FLAGELLIN-RESPONSIVE KINASE1* (*FRK1*) was considerably higher in *aca8 aca10* plants compared to wild type (Figure 4). This could point at elevated MAPK signalling in *aca8 aca10*; however, there was no correlation between flg22-induced MAPK activation and the increased expression of MAPK-specific genes (Figure S7). Induction of the downstream genes cytochrome P450 monooxygenase *CYP81F2*, *FAD-LINKED OXIREDUCTASE* (*FOX*) and *NDR1/HIN-LIKE 10* (*NHL10*) that are controlled by both the MAPK and CDPK pathway were either wild type-like or somewhat enhanced (Figure 4). By contrast, the flg22-induced transcript accumulation of the CDPK downstream gene *PHOSPHATE-INDUCED 1* (*PHI1*) was notably reduced compared to wild-type levels (Figure 4). This indicates that gene induction mediated by CDPK signalling is insufficient, likely due to altered flg22 activation of the CDPK cascade.

Our data show that knock-out of *ACA8 ACA10* function causes pronounced changes in steady-state transcript levels, probably for phenotypic compensation, and also impairs proper flg22-induced transcriptional reprogramming. This was further supported by differential transcript accumulation of additional markers genes (Figure S8), which either was enhanced (*At5g25250*, *At1g66880* and *MYB51/At1g18570*) or reduced upon flg22 elicitation (*At2g47140* and *WRKY30/At5g24110*). We also investigated flg22-dependent expression of *ACA12* and *ACA13*, which are potential candidates for compensating *ACA8* and *ACA10* loss-of-function (Figure S1A). After flg22 treatment, both *ACA12* and *ACA13* transcripts accumulated to higher levels in the *aca8 aca10* double mutant background, whereas no significant differences and a slight up-regulation in *ACA12* and *ACA13* abundance, respectively, were detected without MAMP stimulus (Figure 4). Thus, ACA12 and ACA13

may contribute to control cytosolic Ca^{2+} levels during flg22 responses. Intriguingly, ACA12 localizes to the plasma membrane and can interact with the RKs BRI1 and CLV1 (Figure 1A). ACA12, however, failed to associate with FLS2, which may hamper possible compensatory effects in flg22 responses.

ACA8 and ACA10 contribute to plant immunity

To examine a possible role of ACA8 and ACA10 in plant anti-bacterial immunity, all genotypes were spray-inoculated with virulent *Pseudomonas syringae* pv. *tomato* DC3000 (*Pto*DC3000), an infection that is defeated utilizing the FLS2 pathway (Zipfel et al., 2004). Bacterial growth and disease symptom development were monitored three and five days post inoculation, respectively. *Pto*DC3000 multiplied to high titers in *aca8* and *aca10* single as well as in *aca8 aca10* double mutants, which was comparable to those detected in immune-compromised *fls2* mutants (Figure 5A). This enhanced susceptibility was reduced to wild type levels in the transgenic *ACA8-GFP* complementation line. Moreover, disease symptom development of *aca8* and *aca10* single and double mutants was correlated with the enhanced susceptibility phenotype (Figure 5B). Despite *35S*-driven ectopic expression of *ACA8-GFP*, no increased resistance against *Pto*DC3000 could be detected in the transgenic line. *Aca8* and *aca10* single mutants were as affected as the *aca8 aca10* double mutant upon *Pto*DC3000 infection. Thus, ACA8 and ACA10 both, individually and equally contribute to plant immunity in bacterial infections.

Discussion

It is well known that MAMPs induce a rapid and transient increase of $[Ca^{2+}]$ in the cytosol through the function of plasma membrane resident Ca^{2+} channels (Blume et al., 2000; Ranf et al., 2011), but despite its presumed importance in plant immunity, our current understanding of how the MAMP-induced Ca^{2+} burst is regulated is rather limited (Ranf et al., 2008; Kudla et al., 2010). Though DND1 is important for cytosolic Ca^{2+} elevation in response to bacterial lipopolysaccharides (LPS) and endogenous danger peptides (Ma et al., 2009; Qi et al., 2010), it is not required for flg22 and elf18 activation of Ca^{2+} (Jeworutzki et al., 2010). Similarly, the recently suggested GLR-type Ca^{2+} channels have been implicated in cryptogein- and flg22-triggered responses by pharmacological approaches, however, genetic evidence for their involvement in MAMP signalling is still lacking (Kwaitaal et al., 2011; Michard et al., 2011; Vatsa et al., 2011). Ca^{2+} homeostasis is also controlled through the

function of Ca^{2+} ATPases, and our data show that FLS2 forms a complex with ACA8. It is possible that FLS2 transphosphorylates the Ca^{2+} ATPase to regulate its activity, as ACA10 is differentially phosphorylated upon flg22 treatment (Benschop et al., 2007).

Based on our mutant loss-of-function data, ACA8 and ACA10 co-function to positively regulate the MAMP-induced Ca^{2+} burst. Because of their function as Ca^{2+} pumps, Ca^{2+} ATPases mediate efflux of Ca^{2+} ions out of the cytosol. Therefore, loss of Ca^{2+} ATPase function should result in an enhanced and prolonged Ca^{2+} burst (Romani et al., 2004). In line with this assumption, Ca^{2+} fluxes triggered by the MAMP cryptogein in *N. benthamiana* were increased in amplitude and duration when ER-localized *NbCA1* was silenced (Zhu et al., 2010). Our data on ACA8 and ACA10 unexpectedly revealed a reduction in the MAMP-induced Ca^{2+} burst. We cannot exclude the possibility that other members of the ACA family such as ACA12 and ACA13 may substitute at least partially for ACA8 and ACA10 function in the mutant backgrounds as evidenced by the increased *ACA12* and *ACA13* transcript levels upon flg22 elicitation. This would indicate that the observed phenotypes of *aca8 aca10* mutants are rather an indirect effect. However, ACA12 did not associate with FLS2 in our BiFC analysis, *ACA12* and *ACA13* transcript levels were not generally increased in *aca8 aca10* mutants, and our transcriptome data did not point at obvious expression changes of any other member of the ACA family. Alternatively, it is possible that the enhanced transcript levels of *CaM*-like genes in *aca8 aca10* plants reflect a mechanism to compensate for elevated steady-state levels of cytosolic Ca^{2+}. This may in turn lead to the decreased influx of Ca^{2+} into the cytosol, because CaM-like proteins were shown to regulate cyclic nucleotide-gated channels (CNGCs), a class of cation channels with a documented role in Ca^{2+} influx (Ali et al., 2007; Boursiac and Harper, 2007). CaM-like proteins can also activate Ca^{2+} ATPases and are thus key regulators of Ca^{2+} homeostasis (Boursiac and Harper, 2007). However, we cannot exclude a yet unknown modality of Ca^{2+} ATPase function implying a direct rather than indirect action. Based on current knowledge it is possible to speculate that FLS2 may transiently down-regulate ACA8 and ACA10 activities upon flg22 treatments thereby allowing a cytosolic Ca^{2+} burst, possibly masked by investigating stable loss-of-function mutants.

Flg22-induced ROS production was decreased in *aca8 aca10* mutants, which is in agreement with a reduction of the flg22-triggered Ca^{2+} burst. Likewise, chemical inhibition of Ca^{2+} ATPase function resulted in reduced ROS production in response to the fungal MAMP oligogalacturonide, placing ACA proteins upstream of RbohD (Romani et al., 2004). As Rboh proteins contain two EF hand motifs in their N-terminal domains (Ogasawara et al., 2008), an

altered Ca^{2+} signature in *aca8 aca10* plants may impair ROS generation catalyzed by the NADPH oxidases. In potato, CDPK signalling promotes Rboh-mediated ROS production (Kobayashi et al., 2007). This supports the idea of changed CDPK activation in *aca8 aca10* plants and ACA8/ACA10 regulating kinase signalling, which is substantiated by altered flg22-induced gene expression caused by *ACA8 ACA10* loss-of-function. The MAPK/CDPK differential gene expression shows that the flg22-induced Ca^{2+} burst is required for the concerted activation of the kinase signalling pathways in order to properly reprogram the transcriptome upon MAMP perception.

Ca^{2+} ATPases have also been shown to regulate defence responses by affecting programmed cell death (Nemchinov et al., 2008). Silencing of *NbCA1* causes enhanced hypersensitive response cell death upon tobacco mosaic virus activation of the tobacco N immune receptor (Zhu et al., 2010). Knock-out plants of *ACA4* and *ACA11* display cell death-like lesions similar to that triggered by avirulent pathogens, which was dependent on salicylic acid (SA) accumulation (Boursiac et al., 2010). Cell death-related phenotypes were not observed in *aca8 aca10* plants. Instead, they were supersusceptible to infection with *Pto*DC3000 bacteria. Unlike the observed genetic redundancy between ACA8 and ACA10 in plant development and the partial phenotype observed when monitoring individual flg22 responses, the two members of the Ca^{2+} ATPase family are equally required for plant immunity, with single mutants exhibiting a similar level of susceptibility as *fls2* mutants. This apparent difference may be due to the different time frames measuring early flg22 responses and the endpoint of bacterial infections. Sustained increase of cytosolic Ca^{2+} rather than a transient burst activates downstream defences (Blume et al., 2000). Additionally, other than MAMP responses, pathogen growth depends on multiple layers of basal immunity, e.g. interference of immunity by effectors from *Pto*DC3000. Effectors can target MAMP receptors at the plasma membrane (Block and Alfano, 2011), or effectors could directly affect the molecular components controlling Ca^{2+} fluxes. Alternatively, perception of the complex mixture of different MAMPs present in *Pto*DC3000 may require independent functions of ACA8 and ACA10 or other members of the ACA family. This is supported by the differential expression pattern of *aca8 aca10* de-regulated genes in response to flg22 or oligogalacturonides (Figure S6). Moreover, CaM is implicated as negative regulator in SA-mediated disease resistance, and the CaM binding protein CBP60g contributes to flg22-elicited SA accumulation and anti-bacterial defence (Du et al., 2009; Wang et al., 2009), which demonstrates a role for the ACA8/ACA10 de-regulated *CaM*-like genes in plant immunity.

MAMPs are known to trigger a Ca^{2+} burst, one of the most upstream responses in defence signalling (Boller and Felix, 2009; Segonzac et al., 2011). However, the molecular components underlying the complex regulatory network regulating the Ca^{2+} fluxes are still poorly described. In this study, we identified two plasma membrane Ca^{2+} ATPases, ACA8 and ACA10, which based on mutant loss-of-function data act as positive regulators of early MAMP responses. Our findings further illustrate the importance of coordinated and fine-tuned MAMP responses, including Ca^{2+} signalling, for plant immunity. Given the altered MAMP-induced MAPK-/CDPK-dependent transcriptional changes together with the ACA8-FLS2 complex formation at the plasma membrane, our results suggest a mechanistic link between the receptor complex and signalling kinases *via* the secondary messenger Ca^{2+}. Although root tip growth upon flg22 treatment and in *fls2* mutants remains to be inspected in more detail, our data also suggest a broader function of Ca^{2+} ATPases in RK-mediated signalling. The functional relevance of the interaction of ACA8 and BRI1 is supported by the *aca8 aca10* mutant phenotype showing defects in early differentiation of root stem cells (Clouse and Sasse, 1998; Hacham et al., 2011). BRI1-mediated brassinosteroid signalling has been shown to affect root growth through regulation of the cell cycle (Gonzales-Garcia et al., 2011). Additionally, it is possible that ACA8 and/or ACA10 associate with the Arabidopsis CRINKLY 4 (ACR4) RK, known to regulate root stem cells via the CLV3-related peptide CLE40, in particular as root cell type-specific expression data provide evidence for *ACA10* transcripts accumulate around the stem cell niche (Brady et al., 2007; Winter et al., 2007; De Smet et al., 2008; Stahl et al., 2009). In analogy to the multiple roles of the co-receptor BAK1/SERK3, this places plasma membrane Ca^{2+} ATPases as important components of RK signalling pathways, likely through the regulation of Ca^{2+} fluxes in the cytosol. Dissecting the precise molecular mechanism of the RK- Ca^{2+} ATPase interaction will further advance our understanding of receptor-mediated signal transduction in the future.

Materials and Methods

Plant lines and growth conditions

T-DNA lines for *ACA8* (GK-688H09) and *ACA10* (GK-044H01) were obtained from the European Seed Stock Center NASC (http://arabidopsis.info/), and the tilling *ACA8*^{Q70*} line was obtained from the Seattle Tilling Project (http://tilling.fhcrc.org/). Homozygous insertions of all *aca8, aca10, aca8 aca10, aca8*^{Q70*}, *aca8*^{Q70*} *aca10* mutant plants were validated in the F2 populations by PCR and sequencing. *35S::ACA8-GFP*, *35S::Aequorin*

(*Aeq*) transgenic and *fls2* mutant lines were previously described (Knight et al., 1991; Zipfel et al., 2004; Lee et al., 2007). Homozygous crossed *aca8 aca10 ACA8-GFP*, *aca8 Aeq*, *aca10 Aeq*, *aca8 aca10 Aeq* and *fls2 Aeq* were confirmed by PCR (all oligonucleotides used in this study are summarized in Table S3). Arabidopsis plants grown on soil were kept under short day conditions for 4-5 weeks. Arabidopsis seedlings were *in vitro* grown on plates or liquid containing MS-medium and 1 % sucrose and kept under long day conditions for 10-14 days. *N. benthamina* plants were soil-grown under long day conditions for 4-5 weeks.

Bimolecular fluorescence complementation

FLS2-Yc, FLS2-Yn, BRI1-Yc, BRI1-Yn, CLV1-Yc, CLV1-Yn, ACA8-Yc, ACA8-Yn, ACA12-Yc and ACA12-Yn constructs were made by PCR cloning the corresponding full-length cDNAs using the Gateway technology in the pAMPAT destination vector series, and introduced into *A. tumefaciens* strain GV3101 carrying the p19 silencing suppressor (Voinnet et al., 2003; Lefebvre et al., 2010). Overnight cultures were diluted OD_{600} = 0.1 in water supplemented with 100 μM acetosyringone and inoculated into 4 weeks-old *N. benthamiana* leaves. Leaf samples were imaged at 1 dpi using a Leica confocal TCS SP5 microscope with the Leica LAS AF system software. YFP emission and chlorophyll autofluorescence were detected at emission spectra 520 to 600 nm and 680 to 780 nm, respectively, after excitation at 488 nm. All samples were imaged with the 20x objective. Pictures were taken in line averaging of four scans. Same confocal settings were used to image all samples. Representative images of over three biological replicates are shown.

FRET-FLIM measurements

FLS2-CFP, FLS2-YFP, ACA8-CFP and ACA8-YFP constructs were PCR cloned as the corresponding full-length cDNAs using the Gateway technology in the pCZN575 and pCZN576 vectors, and improved sCFP3A and sYFP2 chromophore variants, respectively (Kremers et al., 2006; Karlova et al., 2011). Constructs were transfected into mesophyll protoplasts from soil-grown Arabidopsis Col-0 plants as described before (Russinova et al., 2004), which were prepared using the tape sandwich method (Wu et al., 2009). FRET-FLIM measurements were performed using the Biorad Radiance 2100 MP system combined with a Nikon TE 300 inverted microscope and a Hamamatsu R3809U MCP PMT (Russinova et al., 2004). FRET between CFP and YFP was detected by monitoring donor emission using a 470-500 nm band pass filter. Images with a frame size of 64 x 64 pixels were acquired and the average count rate was around $0.5x10^4$ photons per second for an acquisition time of ± 120

sec. Donor fluorescence lifetimes (CFP) were analyzed using SPCImage 3.10 software (Becker & Hickl) using a one and two-component decay model. Average fluorescence lifetimes of different combinations in several cells (n>10) along the plasma membrane were calculated (Table S1). Statistical significance of differences between donor only and donor-acceptor combinations was determined using a Student's T-test.

Ca^{2+} measurements

12 days-old sterile grown seedlings in liquid medium were supplied with 100 µl MS medium containing 10 µM coelenterazine (BIOSYNTH, Switzerland) and dark incubated overnight. Seedlings were supplied with fresh 100 µl MS medium and dark incubated for 30 min. Aequorin measurements were performed using the Centro LB960 luminometer system (Berthold Technologies, Germany). Luminescence from single wells was detected over 0.25 sec and each well was measured every 30 sec. After 2 min of measurement, flg22 (EZBiolab, US) and chitin (SIGMA, Germany) were added to final concentrations of 1 µM or 0.1 mg/ml, respectively, and luminescence was measured over 40 min. For calculation of Ca^{2+} concentrations, 100 µl 2 M $CaCl_2$ in 20% ethanol was added and luminescence was measured over 30 min (0.25 sec per well every 63 sec). Ca^{2+} concentrations were calculated according to Rentel and Knight (Rentel and Knight, 2004). Differences in aequorin levels due to transgene expression and seedling size were corrected by calculating Ca^{2+} concentrations and not using luminescence counts. Per treatment 2x8 individual wells were averaged. Ca^{2+} transients were compared between treatments within one experiment unless stated otherwise. Significant differences were evaluated using ANOVA with Tukey-HSD test.

ROS measurements

Leaf discs of five weeks-old plants were used for ROS measurements as previously described (Segonzac et al., 2011). Oxidative burst was elicited with 100 nM flg22 or 100 ug/mL chitin oligosaccharide; a negative control without MAMP elicitation was included in all experiments. Luminescence was measured over time using an ICCD photon-counting camera (Photek).

Biochemical analysis

Western blotting: Proteins were separated on 10 % SDS-PAGE gels, transferred onto PVDF membranes using a semi-dry transfer system followed by blocking in 5 % milk or 3 % BSA. Antibodies were diluted as follows: anti-p42/44 MAPK (Cell Signalling Technology;

1:1000), anti-FLS2 (see (Mersmann et al., 2010); 1:5000) AP-conjugated anti-rabbit (SIGMA; 1:20,000 to 1:30,000). Alkaline-phosphatase activity was detected using the CDP-Star (ROCHE).

MAPK assay: 14 days-old seedlings grown on MS plates were sprayed with 2 μM flg22 for 0, 5, 15 or 60 min before harvest. 100 mg of plant material was ground and solubilised in 200 μL buffer (50 mM Tris-HCl pH 7.5, 150 mM NaCl, 10 % glycerol, 1 mM EDTA, 10 mM NaF, 2 mM NaVO3, 25 mM β-glycerophosphate, 1mM Pefabloc, 1mM DTT, 1 mM PMSF, 0.1 % Tween 20) supplied with 3.4 μL/100 mg FW protease inhibitor cocktail (SIGMA). Extracts were centrifuged, solubilised by 5 min boiling in 2 % SDS Laemmli buffer, and equal amounts were loaded onto SDS gels. MAPK activation was detected with anti-p42/44 MAPK antibodies.

Transcript profiling

For qRT-PCR analysis, 14 days-old sterile grown seedlings were untreated or treated with 1μM flg22 for 1h or 24 h. RNA was extracted and DNA digested using the RNeasy plant mini kit and the RNase-Free DNase Set (QIAGEN, Germany). 2μg of RNA was used to synthesize cDNA using the Superscript II enzyme (INVITROGEN). 1μL of a 10x dilution of the cDNA was used for each quantitative PCR, using a Bio-Rad iQ5 apparatus and SYBR Green I detection. All oligonucleotides used in this study are summarized in Table S3.

Pathogen infection assays

4 weeks-old soil-grown (Jiffy pellets) Arabidopsis plants were surface inoculated with *Pto*DC3000 bacteria at 10^8 colony-forming units mL^{-1} and sampled at 3 dpi. Two leaf disks were pooled from each six individual plants and bacterial extraction was done as described before (Zipfel et al., 2004). The results of three independent experiments were combined and T-test analysis was performed.

Acknowledgements

We thank W.S. Chung (Gyeongsang National University, Korea) for kindly providing the *35S::ACA8-GFP* transgenic line mutant, Marc Knight for the *35S::Aequorin* line, GABI-KAT for T-DNA insertion lines, and the Seattle Tilling Project for the tilling line. We thank A.M.E. Jones, J, Sklenar and S. Laurent for technical help, M. Beck for constructs, U. Goebel and E. Ver Loren van Themaat for data analysis of the Affymetrix Tiling 1.0R array, C. Zipfel for providing materials and advice, T. Romeis for fruitful discussions, and G. Oldroyd for

reading the manuscript. This work was supported by the German Research Council (SFB670) and the Gatsby Charitable Foundation.

Author contributions

N.F.d.F., and S.R. designed research; N.F.d.F., M.M., M.K., L.N., D.A., H.H., R.L.-D., M.F.N., B.H., and J.W.B. performed research; N.F.d.F., M.M., L.N., R.L.-D., T.B., B.H., J.W.B., R.P., and S.R. analysed data; and S.R. wrote the paper.

Competing interests

The authors have declared that no competing interests exist.

References

Albrecht C, Boutrot F, Segonzac C, Schwessinger B, Gimenez-Ibanez S, Chinchilla D, Rathjen JP, de Vries SC, Zipfel C (2012) Brassinosteroids inhibit pathogen-associated molecular pattern-triggered immune signaling independent of the receptor kinase BAK1. Proceedings of the National Academy of Sciences of the United States of America **109:** 303-308

Albrecht C, Russinova E, Kemmerling B, Kwaaitaal M, de Vries SC (2008) Arabidopsis SOMATIC EMBRYOGENESIS RECEPTOR KINASE proteins serve brassinosteroid-dependent and -independent signaling pathways. Plant Physiol **148:** 611-619

Ali R, Ma W, Lemtiri-Chlieh F, Tsaltas D, Leng Q, von Bodman S, Berkowitz GA (2007) Death don't have no mercy and neither does calcium: Arabidopsis CYCLIC NUCLEOTIDE GATED CHANNEL2 and innate immunity. Plant Cell **19:** 1081-1095

Aslam SN, Newman MA, Erbs G, Morrissey KL, Chinchilla D, Boller T, Jensen TT, De Castro C, Ierano T, Molinaro A, Jackson RW, Knight MR, Cooper RM (2008) Bacterial polysaccharides suppress induced innate immunity by calcium chelation. Curr Biol **18:** 1078-1083

Belkhadir Y, Jaillais Y, Epple P, Balsemao-Pires E, Dangl JL, Chory J (2012) Brassinosteroids modulate the efficiency of plant immune responses to microbe-associated molecular patterns. Proceedings of the National Academy of Sciences of the United States of America **109:** 297-302

Benschop JJ, Mohammed S, O'Flaherty M, Heck AJ, Slijper M, Menke FL (2007) Quantitative phosphoproteomics of early elicitor signaling in Arabidopsis. Mol Cell Proteomics **6:** 1198-1214

Block A, Alfano JR (2011) Plant targets for Pseudomonas syringae type III effectors: virulence targets or guarded decoys? Curr Opin Microbiol **14:** 39-46

Blume B, Nurnberger T, Nass N, Scheel D (2000) Receptor-mediated increase in cytoplasmic free calcium required for activation of pathogen defense in parsley. Plant Cell **12:** 1425-1440

Boller T, Felix G (2009) A renaissance of elicitors: perception of microbe-associated molecular patterns and danger signals by pattern-recognition receptors. Annu Rev Plant Biol **60:** 379-406

Bonza MC, Luoni L, De Michelis MI (2004) Functional expression in yeast of an N-deleted form of At-ACA8, a plasma membrane Ca(2+)-ATPase of Arabidopsis thaliana, and characterization of a hyperactive mutant. Planta **218:** 814-823

Bonza MC, Morandini P, Luoni L, Geisler M, Palmgren MG, De Michelis MI (2000) At-ACA8 encodes a plasma membrane-localized calcium-ATPase of Arabidopsis with a calmodulin-binding domain at the N terminus. Plant Physiol **123:** 1495-1506

Boudsocq M, Willmann MR, McCormack M, Lee H, Shan L, He P, Bush J, Cheng SH, Sheen J (2010) Differential innate immune signalling via Ca(2+) sensor protein kinases. Nature **464:** 418-422

Boursiac Y, Harper JF (2007) The origin and function of calmodulin regulated Ca2+ pumps in plants. J Bioenerg Biomembr **39:** 409-414

Boursiac Y, Lee SM, Romanowsky S, Blank R, Sladek C, Chung WS, Harper JF (2010) Disruption of the vacuolar calcium-ATPases in Arabidopsis results in the activation of a salicylic acid-dependent programmed cell death pathway. Plant Physiol **154:** 1158-1171

Bracha-Drori K, Shichrur K, Katz A, Oliva M, Angelovici R, Yalovsky S, Ohad N (2004) Detection of protein-protein interactions in plants using bimolecular fluorescence complementation. The Plant journal : for cell and molecular biology **40:** 419-427

Brady SM, Orlando DA, Lee JY, Wang JY, Koch J, Dinneny JR, Mace D, Ohler U, Benfey PN (2007) A high-resolution root spatiotemporal map reveals dominant expression patterns. Science **318:** 801-806

Chen X, Chern M, Canlas PE, Ruan D, Jiang C, Ronald PC (2010) An ATPase promotes autophosphorylation of the pattern recognition receptor XA21 and inhibits XA21-mediated immunity. Proc Natl Acad Sci U S A **107:** 8029-8034

Chinchilla D, Shan L, He P, de Vries S, Kemmerling B (2009) One for all: the receptor-associated kinase BAK1. Trends Plant Sci **14:** 535-541

Chinchilla D, Zipfel C, Robatzek S, Kemmerling B, Nurnberger T, Jones JD, Felix G, Boller T (2007) A flagellin-induced complex of the receptor FLS2 and BAK1 initiates plant defence. Nature **448:** 497-500

Cho D, Kim SA, Murata Y, Lee S, Jae SK, Nam HG, Kwak JM (2009) De-regulated expression of the plant glutamate receptor homolog AtGLR3.1 impairs long-term Ca2+-programmed stomatal closure. Plant J **58:** 437-449

Clough SJ, Fengler KA, Yu IC, Lippok B, Smith RK, Jr., Bent AF (2000) The Arabidopsis dnd1 "defense, no death" gene encodes a mutated cyclic nucleotide-gated ion channel. Proc Natl Acad Sci U S A **97:** 9323-9328

Clouse SD, Sasse JM (1998) BRASSINOSTEROIDS: Essential Regulators of Plant Growth and Development. Annu Rev Plant Physiol Plant Mol Biol **49:** 427-451

Conn SJ, Gilliham M, Athman A, Schreiber AW, Baumann U, Moller I, Cheng NH, Stancombe MA, Hirschi KD, Webb AA, Burton R, Kaiser BN, Tyerman SD, Leigh RA (2011) Cell-specific vacuolar calcium storage mediated by CAX1 regulates apoplastic calcium concentration, gas exchange, and plant productivity in Arabidopsis. Plant Cell **23:** 240-257

De Smet I, Vassileva V, De Rybel B, Levesque MP, Grunewald W, Van Damme D, Van Noorden G, Naudts M, Van Isterdael G, De Clercq R, Wang JY, Meuli N, Vanneste S, Friml J, Hilson P, Jurgens G, Ingram GC, Inze D, Benfey PN, Beeckman T (2008) Receptor-like kinase ACR4 restricts formative cell divisions in the Arabidopsis root. Science **322:** 594-597

Dodd AN, Kudla J, Sanders D (2010) The language of calcium signaling. Annu Rev Plant Biol **61:** 593-620

Du J, Xie J, Yue L (2009) Intracellular calcium activates TRPM2 and its alternative spliced isoforms. Proc Natl Acad Sci U S A **106:** 7239-7244

Fradin E, Adb-El-Haliem A, Masini L, van den Berg G, Joosten M, Thomma B (2011) Interfamily transfer of tomato Ve1 mediates Verticillium resistance in Arabidopsis. Plant Physiol

George L, Romanowsky SM, Harper JF, Sharrock RA (2008) The ACA10 Ca2+-ATPase regulates adult vegetative development and inflorescence architecture in Arabidopsis. Plant Physiol **146:** 716-728

Hacham Y, Holland N, Butterfield C, Ubeda-Tomas S, Bennett MJ, Chory J, Savaldi-Goldstein S (2011) Brassinosteroid perception in the epidermis controls root meristem size. Development **138:** 839-848

Hwang I, Harper JF, Liang F, Sze H (2000) Calmodulin activation of an endoplasmic reticulum-located calcium pump involves an interaction with the N-terminal autoinhibitory domain. Plant Physiol **122:** 157-168

Irizarry RA, Hobbs B, Collin F, Beazer-Barclay YD, Antonellis KJ, Scherf U, Speed TP (2003) Exploration, normalization, and summaries of high density oligonucleotide array probe level data. Biostatistics **4:** 249-264

Jeworutzki E, Roelfsema MR, Anschutz U, Krol E, Elzenga JT, Felix G, Boller T, Hedrich R, Becker D (2010) Early signaling through the Arabidopsis pattern recognition receptors FLS2 and EFR involves Ca-associated opening of plasma membrane anion channels. Plant J **62:** 367-378

Karlova R, Rosin FM, Busscher-Lange J, Parapunova V, Do PT, Fernie AR, Fraser PD, Baxter C, Angenent GC, de Maagd RA (2011) Transcriptome and metabolite profiling show that APETALA2a is a major regulator of tomato fruit ripening. Plant Cell **23:** 923-941

Keinath NF, Kierszniowska S, Lorek J, Bourdais G, Kessler SA, Shimosato-Asano H, Grossniklaus U, Schulze WX, Robatzek S, Panstruga R (2010) PAMP (Pathogen-associated Molecular Pattern)-induced Changes in Plasma Membrane Compartmentalization Reveal Novel Components of Plant Immunity. Journal of Biological Chemistry **285:** 39140-39149

Knight MR, Campbell AK, Smith SM, Trewavas AJ (1991) Transgenic plant aequorin reports the effects of touch and cold-shock and elicitors on cytoplasmic calcium. Nature **352:** 524-526

Kobayashi M, Ohura I, Kawakita K, Yokota N, Fujiwara M, Shimamoto K, Doke N, Yoshioka H (2007) Calcium-dependent protein kinases regulate the production of reactive oxygen species by potato NADPH oxidase. Plant Cell **19:** 1065-1080

Kremers GJ, Goedhart J, van Munster EB, Gadella TW, Jr. (2006) Cyan and yellow super fluorescent proteins with improved brightness, protein folding, and FRET Forster radius. Biochemistry **45:** 6570-6580

Kudla J, Batistic O, Hashimoto K (2010) Calcium signals: the lead currency of plant information processing. Plant Cell **22:** 541-563

Kwaaitaal M, Huisman R, Maintz J, Reinstadler A, Panstruga R (2011) Ionotropic glutamate receptor (iGluR)-like channels mediate MAMP-induced calcium influx in Arabidopsis thaliana. Biochem J **440:** 355-365

Lamotte O, Gould K, Lecourieux D, Sequeira-Legrand A, Lebrun-Garcia A, Durner J, Pugin A, Wendehenne D (2004) Analysis of nitric oxide signaling functions in tobacco cells challenged by the elicitor cryptogein. Plant Physiol **135:** 516-529

Lee SM, Kim HS, Han HJ, Moon BC, Kim CY, Harper JF, Chung WS (2007) Identification of a calmodulin-regulated autoinhibited Ca2+-ATPase (ACA11) that is localized to vacuole membranes in Arabidopsis. FEBS Lett **581:** 3943-3949

Lefebvre B, Timmers T, Mbengue M, Moreau S, Herve C, Toth K, Bittencourt-Silvestre J, Klaus D, Deslandes L, Godiard L, Murray JD, Udvardi MK, Raffaele S, Mongrand S, Cullimore J, Gamas P, Niebel A, Ott T (2010) A remorin protein interacts with symbiotic receptors and regulates bacterial infection. Proc Natl Acad Sci U S A **107:** 2343-2348

Lu H, Rate DN, Song JT, Greenberg JT (2003) ACD6, a novel ankyrin protein, is a regulator and an effector of salicylic acid signaling in the Arabidopsis defense response. Plant Cell **15:** 2408-2420

Ma W, Smigel A, Verma R, Berkowitz GA (2009) Cyclic nucleotide gated channels and related signaling components in plant innate immunity. Plant Signal Behav **4:** 277-282

McCormack E, Tsai YC, Braam J (2005) Handling calcium signaling: Arabidopsis CaMs and CMLs. Trends Plant Sci **10:** 383-389

Mersmann S, Bourdais G, Rietz S, Robatzek S (2010) Ethylene Signaling Regulates Accumulation of the FLS2 Receptor and Is Required for the Oxidative Burst Contributing to Plant Immunity. Plant Physiology **154:** 391-400

Michard E, Lima PT, Borges F, Silva AC, Portes MT, Carvalho JE, Gilliham M, Liu LH, Obermeyer G, Feijo JA (2011) Glutamate receptor-like genes form Ca2+ channels in pollen tubes and are regulated by pistil D-serine. Science **332:** 434-437

Naouar N, Vandepoele K, Lammens T, Casneuf T, Zeller G, van Hummelen P, Weigel D, Ratsch G, Inze D, Kuiper M, De Veylder L, Vuylsteke M (2009) Quantitative RNA expression analysis with Affymetrix Tiling 1.0R arrays identifies new E2F target genes. Plant J **57:** 184-194

Nemchinov LG, Shabala L, Shabala S (2008) Calcium efflux as a component of the hypersensitive response of Nicotiana benthamiana to Pseudomonas syringae. Plant Cell Physiol **49:** 40-46

Ogasawara Y, Kaya H, Hiraoka G, Yumoto F, Kimura S, Kadota Y, Hishinuma H, Senzaki E, Yamagoe S, Nagata K, Nara M, Suzuki K, Tanokura M, Kuchitsu K (2008) Synergistic activation of the Arabidopsis NADPH oxidase AtrbohD by Ca2+ and phosphorylation. J Biol Chem **283:** 8885-8892

Postel S, Kufner I, Beuter C, Mazzotta S, Schwedt A, Borlotti A, Halter T, Kemmerling B, Nurnberger T (2010) The multifunctional leucine-rich repeat receptor kinase BAK1 is implicated in Arabidopsis development and immunity. Eur J Cell Biol **89:** 169-174

Qi Z, Verma R, Gehring C, Yamaguchi Y, Zhao Y, Ryan CA, Berkowitz GA (2010) Ca2+ signaling by plant Arabidopsis thaliana Pep peptides depends on AtPepR1, a receptor with guanylyl cyclase activity, and cGMP-activated Ca2+ channels. Proc Natl Acad Sci U S A **107:** 21193-21198

Ranf S, Eschen-Lippold L, Pecher P, Lee J, Scheel D (2011) Interplay between calcium signalling and early signalling elements during defence responses to microbe- or damage-associated molecular patterns. Plant J

Ranf S, Wunnenberg P, Lee J, Becker D, Dunkel M, Hedrich R, Scheel D, Dietrich P (2008) Loss of the vacuolar cation channel, AtTPC1, does not impair Ca2+ signals induced by abiotic and biotic stresses. Plant J **53:** 287-299

Rentel MC, Knight MR (2004) Oxidative stress-induced calcium signaling in Arabidopsis. Plant Physiol **135:** 1471-1479

Romani G, Bonza MC, Filippini I, Cerana M, Beffagna N, De Michelis MI (2004) Involvement of the plasma membrane Ca2+-ATPase in the short-term response of Arabidopsis thaliana cultured cells to oligogalacturonides. Plant Biol (Stuttg) **6:** 192-200

Roux M, Schwessinger B, Albrecht C, Chinchilla D, Jones A, Holton N, Malinovsky FG, Tor M, de Vries S, Zipfel C (2011) The arabidopsis leucine-rich repeat receptor-like kinases BAK1/SERK3 and BKK1/SERK4 are required for innate immunity to Hemibiotrophic and Biotrophic pathogens. Plant Cell **23:** 2440-2455

Russinova E, Borst JW, Kwaaitaal M, Cano-Delgado A, Yin Y, Chory J, de Vries SC (2004) Heterodimerization and endocytosis of Arabidopsis brassinosteroid receptors BRI1 and AtSERK3 (BAK1). Plant Cell **16:** 3216-3229

Schiott M, Romanowsky SM, Baekgaard L, Jakobsen MK, Palmgren MG, Harper JF (2004) A plant plasma membrane Ca2+ pump is required for normal pollen tube growth and fertilization. Proc Natl Acad Sci U S A **101:** 9502-9507

Schulze B, Mentzel T, Jehle AK, Mueller K, Beeler S, Boller T, Felix G, Chinchilla D (2010) Rapid Heteromerization and Phosphorylation of Ligand-activated Plant Transmembrane Receptors and Their Associated Kinase BAK1. Journal of Biological Chemistry **285:** 9444-9451

Schwessinger B, Roux M, Kadota Y, Ntoukakis V, Sklenar J, Jones A, Zipfel C (2011) Phosphorylation-Dependent Differential Regulation of Plant Growth, Cell Death, and Innate Immunity by the Regulatory Receptor-Like Kinase BAK1. PLoS Genet **7:** e1002046

Segonzac C, Feike D, Gimenez-Ibanez S, Hann DR, Zipfel C, Rathjen JP (2011) Hierarchy and roles of pathogen-associated molecular pattern-induced responses in Nicotiana benthamiana. Plant Physiol **156:** 687-699

Shiu SH, Bleecker AB (2001) Receptor-like kinases from Arabidopsis form a monophyletic gene family related to animal receptor kinases. Proc Natl Acad Sci U S A **98:** 10763-10768

Smyth GK (2004) Linear models and empirical bayes methods for assessing differential expression in microarray experiments. Stat Appl Genet Mol Biol **3:** Article3

Stahl Y, Wink RH, Ingram GC, Simon R (2009) A signaling module controlling the stem cell niche in Arabidopsis root meristems. Current biology : CB **19:** 909-914

Vatsa P, Chiltz A, Bourque S, Wendehenne D, Garcia-Brugger A, Pugin A (2011) Involvement of putative glutamate receptors in plant defence signaling and NO production. Biochimie

Voinnet O, Rivas S, Mestre P, Baulcombe D (2003) An enhanced transient expression system in plants based on suppression of gene silencing by the p19 protein of tomato bushy stunt virus. Plant J **33:** 949-956

Waites R, Simon R (2000) Signaling cell fate in plant meristems. Three clubs on one tousle. Cell **103:** 835-838

Wang L, Tsuda K, Sato M, Cohen JD, Katagiri F, Glazebrook J (2009) Arabidopsis CaM binding protein CBP60g contributes to MAMP-induced SA accumulation and is involved in disease resistance against Pseudomonas syringae. PLoS Pathog **5:** e1000301

Wang X, Kota U, He K, Blackburn K, Li J, Goshe MB, Huber SC, Clouse SD (2008) Sequential transphosphorylation of the BRI1/BAK1 receptor kinase complex impacts early events in brassinosteroid signaling. Dev Cell **15:** 220-235

Wendehenne D, Lamotte O, Frachisse JM, Barbier-Brygoo H, Pugin A (2002) Nitrate efflux is an essential component of the cryptogein signaling pathway leading to defense responses and hypersensitive cell death in tobacco. Plant Cell **14:** 1937-1951

Winter D, Vinegar B, Nahal H, Ammar R, Wilson GV, Provart NJ (2007) An "Electronic Fluorescent Pictograph" browser for exploring and analyzing large-scale biological data sets. PLoS ONE **2:** e718

Wu FH, Shen SC, Lee LY, Lee SH, Chan MT, Lin CS (2009) Tape-Arabidopsis Sandwich - a simpler Arabidopsis protoplast isolation method. Plant Methods **5:** 16

Zhu X, Caplan J, Mamillapalli P, Czymmek K, Dinesh-Kumar SP (2010) Function of endoplasmic reticulum calcium ATPase in innate immunity-mediated programmed cell death. EMBO J **29:** 1007-1018

Zipfel C (2009) Early molecular events in PAMP-triggered immunity. Curr Opin Plant Biol **12:** 414-420

Zipfel C, Robatzek S, Navarro L, Oakeley EJ, Jones JD, Felix G, Boller T (2004) Bacterial disease resistance in Arabidopsis through flagellin perception. Nature **428:** 764-767

Figure Legends

Figure 1. FLS2 interacts with ACA8 *in planta*. A. Bimolecular fluorescence complementation. Representative micrographs show YFP signals of epidermal cells from *N. benthamiana* leaves transformed with plasmids coding for the indicated constructs. N-terminal YFP fragment = YFPn; C-terminal YFP fragment = YFPc. Scale bar = 100 µm. **B.** FRET-FLIM measurements. Micrographs show representative false colour-coded fluorescence lifetime images of Arabidopsis protoplasts transfected with plasmids coding for the indicated constructs. Lower fluorescence lifetimes indicate proximity of the two fluorescence proteins. Scale bar = 2 µm. Similar results were obtained at least in three independent experiments.

Figure 2. ACA8 and ACA10 have a role in plant development. Photographs presenting growth-related phenotypes of the indicated genotypes in Col-0 background (see Figure S1). **A.** Inflorescence growth of eight weeks-old plants. **B.** Rosette leaves of four weeks-old plants. **C.** Root growth of seven day-old *in vitro*-grown seedlings.

Figure 3. Early MAMP responses are altered in *aca8 aca10* mutants. A. Ca^{2+} burst in response to flg22 and chitin. The *Aequorin* (*Aeq*) Ca^{2+} biosensor was introduced into all indicated genotypes. Data were calculated from curves normalized to steady state cytosolic $[Ca^{2+}]$. Presented is the average $\Delta[Ca^{2+}]$ in the peak between 4-5.5 min after elicitation, which was averaged over two independent biological replicates. Error bars indicate standard deviations based on n = 14-16 samples, letters indicate significant differences at $p<0.05$ based on ANOVA Tukey-HSD test. **B.** ROS burst in response to flg22 and chitin. ROS generation (indicated as total photon counts measured between 2-30 min upon elicitation) was monitored over time. Error bars indicate standard deviations based on n = 28 samples, letters indicate significant differences at $p<0.05$ based on T-test. Similar results were obtained at least in two independent experiments. **C**. FLS2 protein levels of the indicated genotypes revealed by western blot. Coomassie staining (CBB) is included as loading control. Similar results were obtained at least in two independent experiments.

Figure 4. Flg22-induced gene expression. Quantitative real-time PCR monitoring transcript levels of flg22-regulated genes and other Ca^{2+} ATPases in the indicated genotypes upon flg22 elicitation. Actin was used as control. Error bars indicate standard deviations based on n = 3 biological experiments with three technical replicates each; asterisks indicate significant

differences between Col-0 and *aca8 aca10* at $p<0.05$ (*) and $p<0.01$ (**) based on Student´s T-test.

Figure 5. ACA8 and ACA10 contribute to plant immunity. A. Bacterial titres (*Pto*DC3000) in the indicated genotypes (four week-old plants) at 3 dpi. Error bars indicate standard deviations of combined three independent biological replicates with each six technical replicates; letters indicate significant differences at $p<0.05$ based on T-test. **B.** Representative photographs showing macroscopic disease symptoms of four week-old plants infected with *Pto*DC3000 at 5 dpi.

Supporting Information

Figure S1. Characterization of *ACA8* and *ACA10* loss-of-function lines. **A.** The family of autoinhibited Ca^{2+} ATPases (ACAs) in Arabidopsis; phylogenetic tree adapted from Baxter et al., 2003. Subcellular localization of ACA proteins is indicated when known. **B.** Intron-exon structure of *ACA8* and *ACA10*. Arrowheads indicate the positions of the T-DNA insertions; the arrow indicates the position of the point mutation leading to the Q70* mutation in *ACA8*. Grey boxes, un-translated regions; white boxes, exons. **C.** RT-PCR confirmation of *aca8* and *aca10* knock-out alleles as well as an *aca8 aca10 ACA8-GFP* complemented line.

Figure S2. Identification of ACA8 and ACA10 peptides by mass-spectrometry analysis of immuno-purified FLS2-GFP. 21 *in vitro* grown seedlings were used either untreated or treated with flg22. Sample preparations, immuno-purifications and MS/MS analysis were performed essentially as described in Roux et al. (2011). Briefly, immuno-purifications of GFP-tagged proteins were done using the magnetic GFP-trap system from Miltenyi Biotech using an IGEPAL-solubilised protein extract (4 mg protein per mL). Beads were washed with 0.1% IGEPAL extraction buffer prior to elution in boiling Laemli buffer. **A.** Peptide coverage of ACA8 and ACA10 proteins identified in an FLS2-GFP immuno-purified complex. Peptides found in untreated samples are highlighted in green, peptides found in flg22-elicited samples are in orange, peptides found in both conditions are indicated in blue, peptides found in all biological replicates of untreated and treated samples are shown in bold. **B.** Tryptic peptides identified by HPLC-electrospray ionization-MS/MS analysis. Peptides occurring in all biological replicates are marked in bold. Reproducibility ([a]) of specific tryptic peptides out of three biological replicates of untreated or flg22-treated samples prepared from Arabidopsis plants expressing FLS2-GFP. In brackets, no peptides were detected in technical controls using wild-type plants (n=2) or plants expressing a plasma membrane addressed GFP (Lti6b-GFP; n=1).

Figure S3. Developmental phenotypes of *aca* mutant plants. **A.** Photographs present inflorescence height and root growth of the indicated genotypes including the tilling allele $aca8^{Q70*}$. **B.** Measurement of primary root growth of 8 days old seedlings, and **C.** number of lateral roots per cm primary root of 14 days old *in vitro*-grown seedlings of the indicated genotypes. Error bars indicate standard error based on n = 25 samples, asterisks indicate significant differences at $p<0.01$ based on T-test. **D.** Detailed view on the stem cell area of

Col-0 wild type and *aca8 aca10* mutant root apical meristems, 3 days after germination. Starch granules in columella cells are visible as pink dots. Note the presence of starch granules in columella stem cells in the *aca8 aca10* meristem (arrow) as sign of perturbation of stem cell identity. For root phenotypic analysis, starch granules in the columella root cap were visualized with 1% Lugol solution (MERC, Germany). Seedlings were stained for 3 min, rinsed with water, cleared with chloral hydrate and analyzed using differential interference contrast optics on a Olympus BX53 light microscope and imaged using a Nikon DS-Fi1 digital camera (Lee et al., 2007).

Figure S4. A. Steady-state Ca^{2+} levels before flg22-triggered Ca^{2+} burst and **B.** after the burst. Data were calculated from the absolute cytosolic [Ca^{2+}] before and at 38 min after elicitation and were averaged over two independent biological replicates. Error bars indicate standard deviations based on n = 14-16 samples, letters indicate significant differences at $p<0.05$ based on ANOVA Tukey-HSD test. Similar results were obtained at least in two independent experiments.

Figure S5. Patterns of the Ca^{2+} burst induced by flg22 (**A**) and chitin (**B**) over time. Included are two *aca8 aca10* lines from independent crosses showing similar results. Curves normalized to steady state cytosolic [Ca^{2+}] show Δ[Ca^{2+}] after MAMP-treatments of one representative biological experiment. Error bars show standard deviations based on n = 6-8 samples. Similar results were obtained at least in two independent experiments.

Figure S6. Altered gene expression in *aca8 aca10* mutants. Overlap of genes up-regulated (A) and down-regulated (B) in *aca8 aca10* and upon elicitation with flg22 and oligogalacturonides (OG). Genes represented show at least two-fold regulation ($p<0.05$) within 1 hr after MPMP treatment according to Denoux et al. (2008). Nine *aca8 aca10* de-regulated genes were removed from the analysis because they were not present in the Denoux et al. (2008) study. The tool used for the Venn diagrams is available at "Venny" http://bioinfogp.cnb.csic.es/tools/venny/index.html. **C.** Flg22-induced CPK5- and CPK11-dependent expression of *aca8 aca10* de-regulated genes (asterisks) according to Boudsocq et al. (2010).

Figure S7. Protein kinase activation in flg22 signalling. MAPK activation upon flg22 application over time. Coomassie staining (CBB) is included as loading control. Similar results were obtained in at least two independent experiments.

Figure S8. Expression analysis of defence marker genes. Quantitative real-time PCR monitoring transcript levels of the indicated genes in Col-0, *aca8 aca10* and *aca8 aca10 ACA8-GFP* plants. Genes in this analysis were not included by Boudsocq et al. (2010). Actin was used as control. Error bars indicate standard deviations based on n = 3 biological experiments with each three technical replicates; asterisks indicate significant differences between Col-0 and *aca8 aca10* at $p<0.05$ (*) and $p<0.01$ (**) based on Student´s T-test.

Table S1. Fluorescence lifetime analysis of the FLS2-ACA8 interaction. Student's T-test was performed comparing donor only (CFP protein fusion) to cells expressing donor and acceptor (YFP protein fusion).

Table S2. Microarray expression data of *aca8 aca10* de-regulated genes. For Affymetrix Tiling 1.0R array analysis, seedlings were grown sterile for 7 days on plates (1/2 MS, 1% sucrose) under short day conditions. A total of three biological replicates each representing approximately 50 seedlings were analysed. RNA was extracted using the RNeasy Plant Mini Kit (QIAGEN, Germany) and qualitatively checked using an Agilent 2100 Bioanalyzer. Hybridization and data analysis were performed as described before (Naouar et al., 2009). In brief, probe-level data were pre-processed using the RMA algorithm (Irizarry et al., 2003), which involves three steps: (i) background correction – where an error component of the intensities is estimated and eliminated; (ii) quantile normalization – where every slide is normalized to have the same cumulative frequency distribution; and (iii) summarization, using the median polish algorithm – where the median values per probe set, adjusted for slide differences, are calculated. On the basis of an empirical Bayes moderated t-statistic for the contrasts (Smyth, 2004), as implemented in the Bioconductor package limma, p-values were calculated and then transformed into false-discovery rates (FDR). The false discovery rate (FDR) control is used in multiple hypothesis testing to correct for multiple comparisons. In a list of rejected hypotheses, FDR controls the expected proportion of incorrectly rejected null hypotheses (type I errors). Data can be accessed from Genbank. Quantitative real-time PCR was used to validate a selection of differentially regulated genes in *aca8 aca10*. Actin was used as control. Fold change expression between Col-0 and *aca8 aca10* +/- standard

deviation (n = 3 biological repeats) is indicated. All genes tested are significantly differentially expressed (Student's T-test : $p < 0.05$) unless for AT5G64870.

Table S3. List of all oligonucleotides used in this study.

Figure 1.

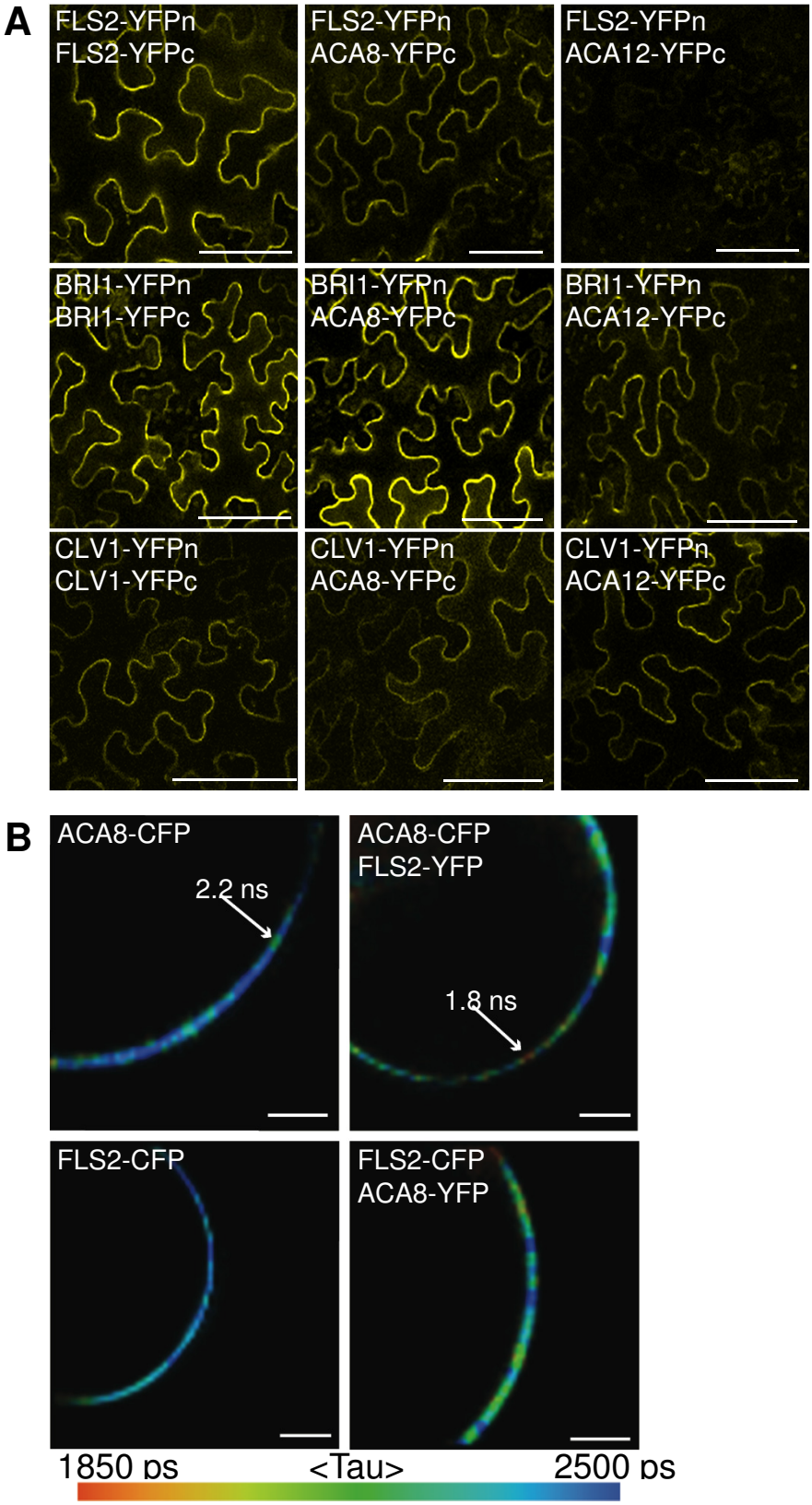

Figure 1. FLS2 interacts with ACA8 *in planta*. A. Bimolecular fluorescence complementation. Representative micrographs show YFP signals of epidermal cells from *N. benthamiana* leaves transformed with plasmids coding for the indicated constructs. N-terminal YFP fragment = YFPn; C-terminal YFP fragment = YFPc. Scale bar = 100 µm. **B.** FRET-FLIM measurements. Micrographs show representative false colour-coded fluorescence lifetime images of Arabidopsis protoplasts transfected with plasmids coding for the indicated constructs. Lower fluorescence lifetimes indicate proximity of the two fluorescence proteins. Scale bar = 2 µm. Similar results were obtained at least in three independent experiments.

Figure 2.

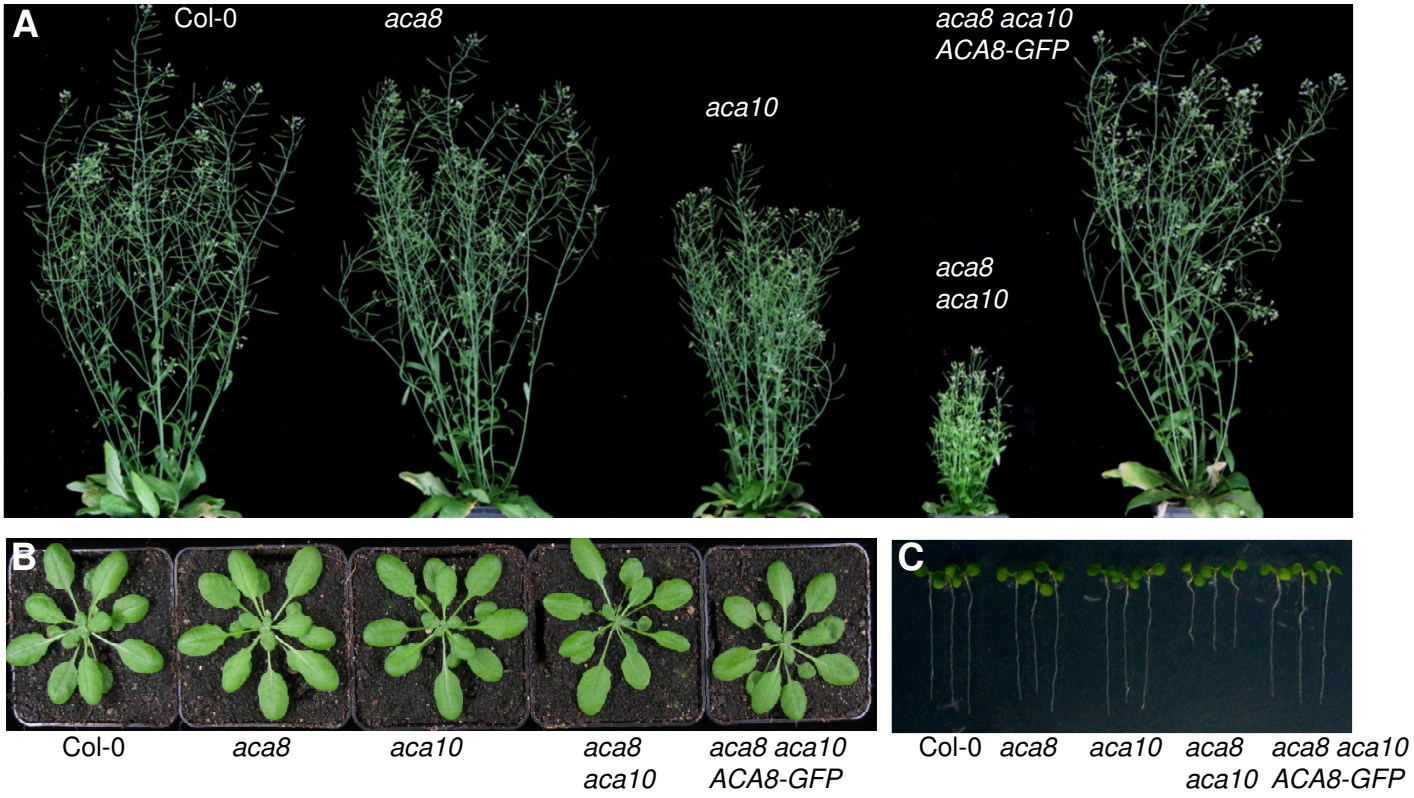

Figure 2. ACA8 and ACA10 have a role in plant development. Photographs presenting growth-related phenotypes of the indicated genotypes in Col-0 background (see Figure S1). **A.** Inflorescence growth of eight weeks-old plants. **B.** Rosette leaves of four weeks-old plants. **C.** Root growth of seven day-old *in vitro*-grown seedlings.

Figure 3.

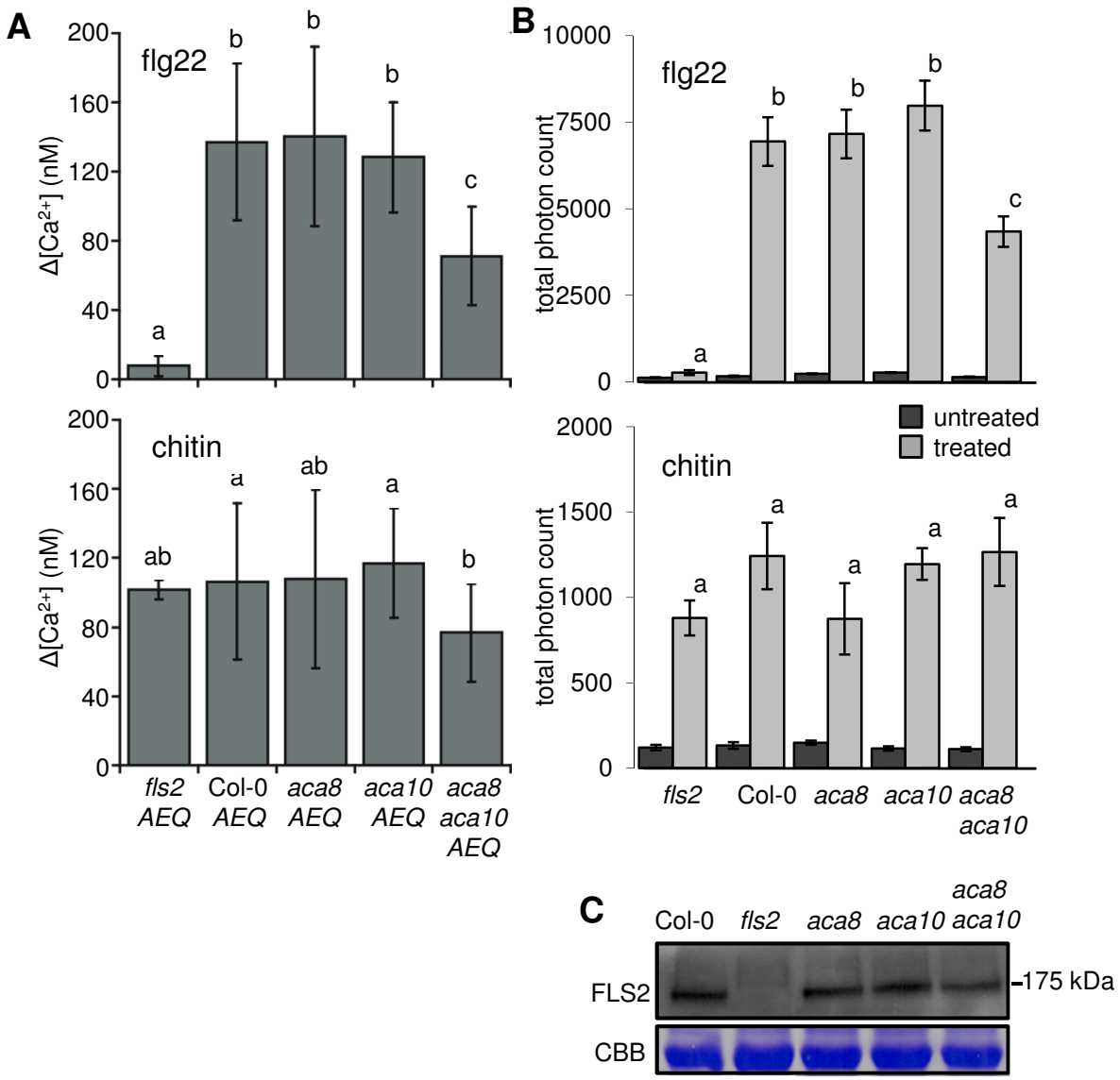

Figure 3. Early MAMP responses are altered in *aca8 aca10* mutants. A. Ca^{2+} burst in response to flg22 and chitin. The *Aequorin* (*Aeq*) Ca^{2+} biosensor was introduced into all indicated genotypes. Data were calculated from curves normalized to steady state cytosolic $[Ca^{2+}]$. Presented is the average $\Delta[Ca^{2+}]$ in the peak between 4-5.5 min after elicitation, which was averaged over two independent biological replicates. Error bars indicate standard deviations based on n = 14-16 samples, letters indicate significant differences at $p<0.05$ based on ANOVA Tukey-HSD test. **B.** ROS burst in response to flg22 and chitin. ROS generation (indicated as total photon counts measured between 2-30 min upon elicitation) was monitored over time. Error bars indicate standard deviations based on n = 28 samples, letters indicate significant differences at $p<0.05$ based on T-test. Similar results were obtained at least in two independent experiments. **C**. FLS2 protein levels of the indicated genotypes revealed by western blot. Coomassie staining (CBB) is included as loading control. Similar results were obtained at least in two independent experiments.

Figure 4.

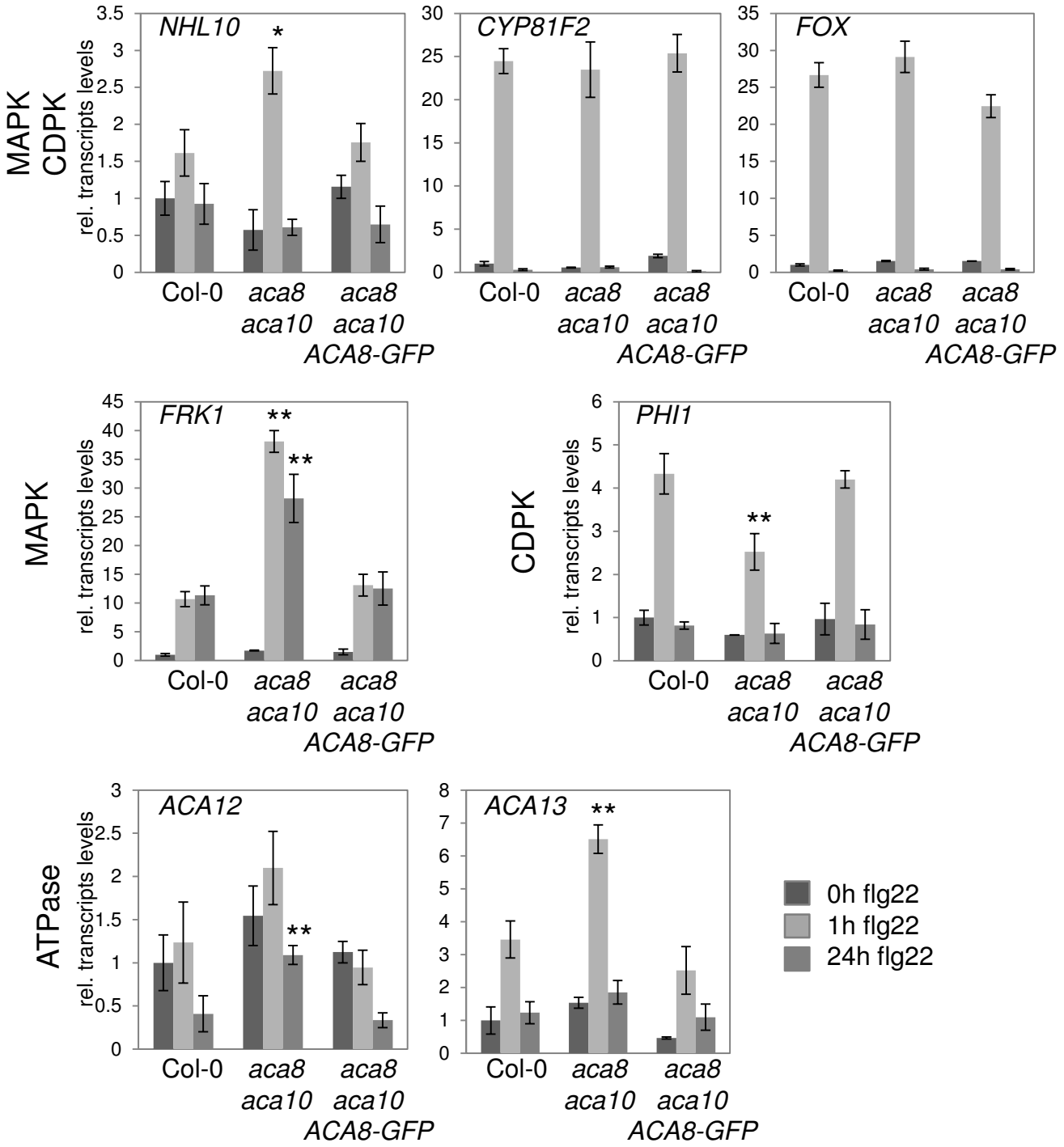

Figure 4. Flg22-induced gene expression. Quantitative real-time PCR monitoring transcript levels of flg22-regulated genes and other Ca^{2+} ATPases in the indicated genotypes upon flg22 elicitation. Actin was used as control. Error bars indicate standard deviations based on n = 3 biological experiments with three technical replicates each; asterisks indicate significant differences between Col-0 and *aca8 aca10* at $p<0.05$ (*) and $p<0.01$ (**) based on Student´s T-test.

Figure 5.

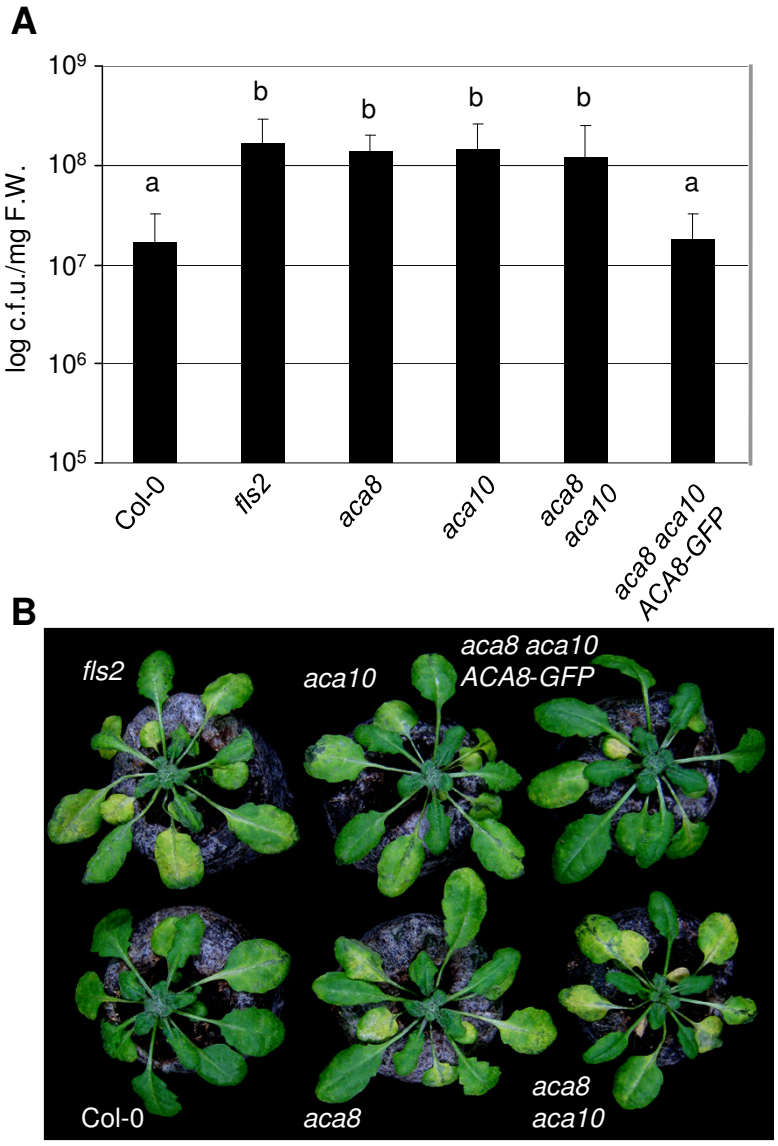

Figure 5. ACA8 and ACA10 contribute to plant immunity. A. Bacterial titres (*Pto*DC3000) in the indicated genotypes (four week-old plants) at 3 dpi. Error bars indicate standard deviations of combined three independent biological replicates with each six technical replicates; letters indicate significant differences at $p<0.05$ based on T-test. **B.** Representative photographs showing macroscopic disease symptoms of four week-old plants infected with *Pto*DC3000 at 5 dpi.

Supplementary figure 1.

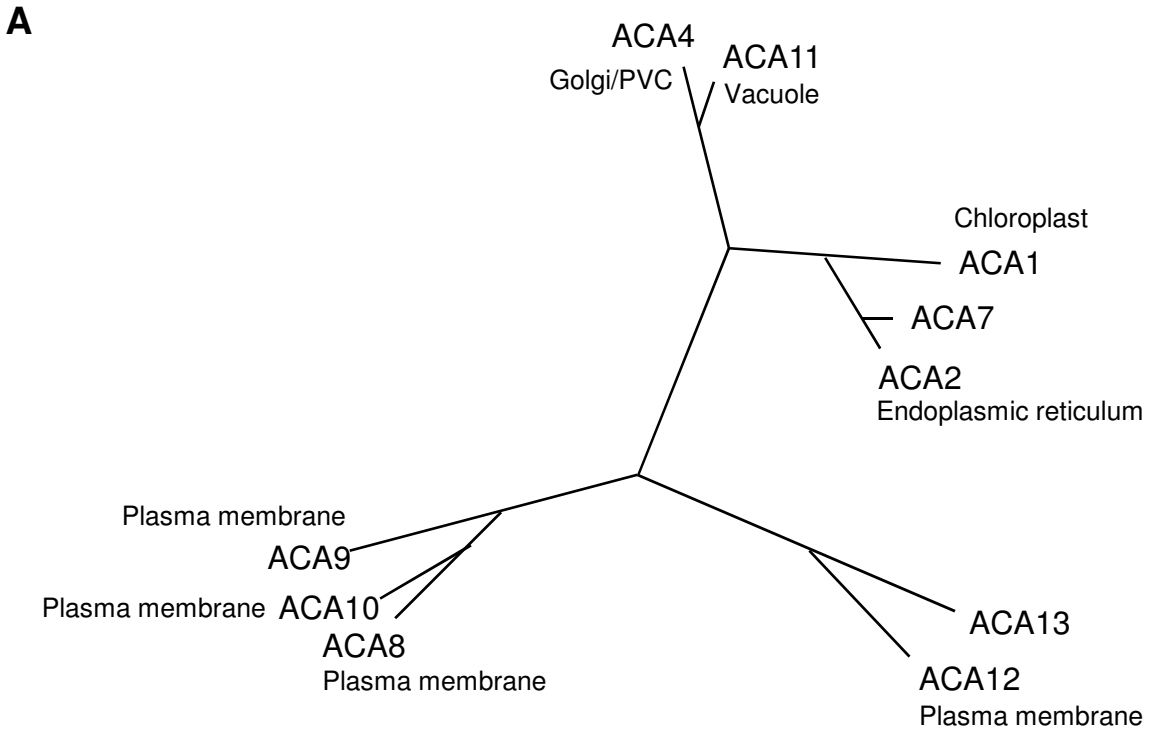

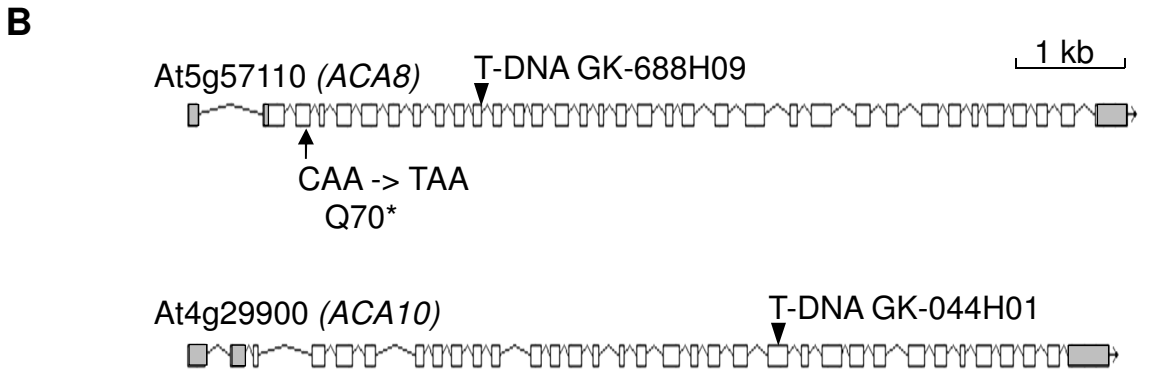

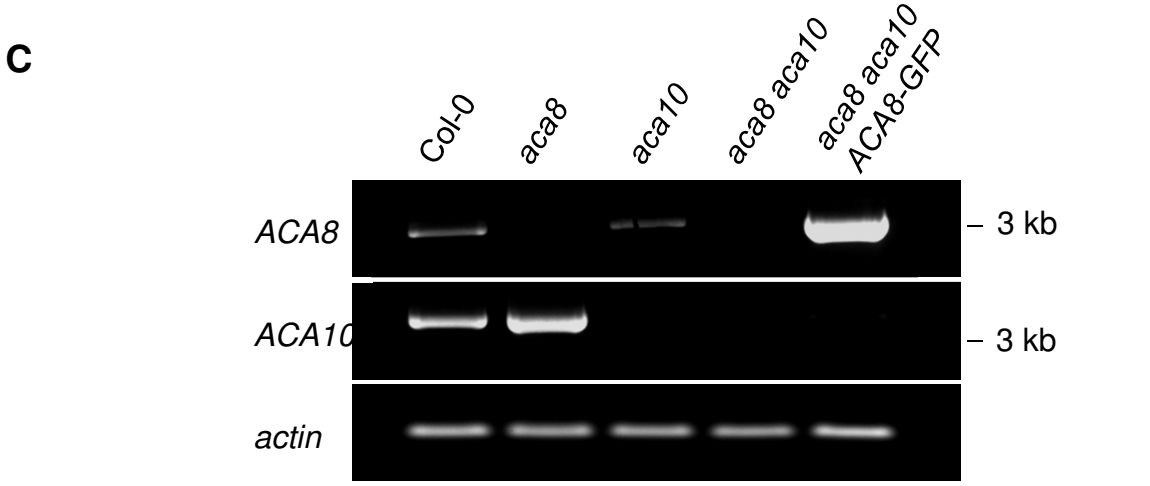

Figure S1. Characterization of *ACA8* and *ACA10* loss-of-function lines. **A.** The family of autoinhibited Ca^{2+} ATPases (ACAs) in Arabidopsis; phylogenetic tree adapted from Baxter et al., 2003. Subcellular localization of ACA proteins is indicated when known. **B**. Intron-exon structure of *ACA8* and *ACA10*. Arrowheads indicate the positions of the T-DNA insertions; the arrow indicates the position of the point mutation leading to the Q70* mutation in *ACA8*. Grey boxes, un-translated regions; white boxes, exons. **C**. RT-PCR confirmation of aca8 and aca10 knock-out alleles as well as an aca8 aca10 ACA8-GFP complemented line.

Supplementary figure 2.

A

ACA8

MTSLLKSSPGRRRGGDVESGKSEHADSDSDTFYIPSKNASIERLQQWRKAALVLNASRRFRYTLDLKKEQE
TREMRQKIRSHAHALLAANRFMDMGRESGVEKTTGPATPAGDFGITPEQLVIMSKDHNSGALEQYGGTQGL
ANLLKTNPEKGISGDDDDLLKRKTIYGSNTYPRKKGKGFLRFLWDACHDLTLIILMVAAVASLALGIKTEG
IKEGWYDGGSIAFAVILVIVVTAVSDYKQSLQFQNLNDEKRNIHLEVLRGGRRVEISIYDIVVGDVIPLNI
GNQVPADGVLISGHSLALDESSMTGESKIVNKDANKDPFLMSGCKVADGNGSMLVTGVGVNTEWGLLMASI
SEDNGEETPLQVRLNGVATFIGSIGLAVAAAVLVILLTRYFTGHTKDNNGGPQFVKGKTKVGHVIDDVVKV
LTVAVTIVVVAVPEGLPLAVTLTLAYSMRKMMADKALVRRLSACETMGSATTICSDKTGTLTLNQMTVVES
YAGGKKTDTEQLPATITSLVVEGISQNTTGSIFVPEGGGDLEYSGSPTEKAILGWGVK|LGMNFETARSQS
SILHAFPFNSEKKRGGVAVKTADGEVHVHWKGASEIVLASCRSYIDEDGNVAPMTDDKASFFKNGINDMAG
RTLRCVALAFRTYEAEKVPTGEELSKWVLPEDDLILLAIVGIKDPCRPGVKDSVVLCQNAGVKVRMVTGDN
VQTARAIALECGILSSDADLSEPTLIEGKSFREMTDAERDKISDKISVMGRSSPNDKLLLVQSLRRQGHVV
AVTGDGTNDAPALHEADIGLAMGIAGTEVAKESSDIIILDDNFASVVKVVRWGRSVYANIQKFIQFQLTVN
VAALVINVVAAISSGDVPLTAVQLLWVNLIMDTLGALALATEPPTDHLMGRPPVGRKEPLITNIMWRNLLI
QAIYQVSVLLTLNFRGISILGLEHEVHEHATRVKNTIIFNAFVLCQAFNEFNARKPDEKNIFKGVIKNRLF
MGIIVITLVLQVIIVEFLGKFASTTKLNWKQWLICVGIGVISWPLALVGKFIPVPAAPISNKLKVLKFWGK
KKNSSGEGSL

ACA10

MSGQFNNSPRGEDKDVEAGTSSFTEYEDSPFDIASTKNAPVERLRRWRQAALVLNASRRFRYTLDLKREED
KKQMLRKMRAHAQAIRAAHLFKAAASRVTGIASPLPTPGGGDFGIGQEQIVSISRDQNIGALQELGGVRGL
SDLLKTNLEKGIHGDDDDILKRKSAFGSNTYPQKKGRSFWRFVWEASQDLTLIILIVAAVASLALGIKTEG
IEKGWYDGISIAFAVLLVIVVTATSDYRQSLQFQNLNEEKRNIRLEVTRDGRRVEISIYDIVVGDVIPLNI
GDQVPADGVLVAGHSLAVDESSMTGESKIVQKNSTKHPFLMSGCKVADGNGTMLVTGVGVNTEWGLLMASV
SEDNGGETPLQVRLNGVATFIGIVGLTVAGVVLFVLVVRYFTGHTKNEQGGPQFIGGKTKFEHVLDDLVEI
FTVAVTIVVVAVPEGLPLAVTLTLAYSMRKMMADKALVRRLSACETMGSATTICSDKTGTLTLNEMTVVEC
YAGLQKMDSPDSSSKLPSAFTSILVEGIAHNTTGSVFR|**SESGEIQVSGSPTER**AILNWAIKLGMDFDALK
SESSAVQFFPFNSEKKRGGVAVKSPDSSVHIHWKGAAEIVLGSCTHYMDESESFVDMSEDKMGGLKDAIDD
MAARSLRCVAIAFRTFEADKIPTDEEQLSRWELPEDDLILLAIVGIKDPCRPGVKNSVLLCQQAGVKVRMV
TGDNIQTAK|AIALECGILASDSDASEPNLIEGKVFRSYSEEERDRICEEISVMGRSSPNDKLLLVQSLKR
RGHVVAVTGDGTNDAPALHEADIGLAMGIQGTEVAKEKSDIIILDDNFESVVKVVRWGRSVYANIQKFIQF
QLTVNVAALVINVVAAISAGEVPLTAVQLLWVNLIMDTLGALALATEPPTDHLMDRAPVGRREPLITNIMW
RNLFIQAMYQVTVLLILNFRGISILHLKSKPNAERVKNTVIFNAFVICQVFNEFNAR|KPDEINIFRGVLR
NHLFVGIISITIVLQVVIVEFLGTFASTTKLDWEMWLVCIGIGSISWPLAVIGKLIPVPETPVSQYFRINR
WRRNSSG

B

protein	peptide sequence	*n* peptide	occurrence[a]	best mascot score
ACA8				
	SHAHALLAANR	4	2/6 - (0/3)	66.4
	DHNSGALEQYGGTQGLANLLK	1	1/6 - (0/3)	43.1
	GISGDDDDLLK	1	1/6 - (0/3)	39.3
	NIHLEVLR	3	3/6 - (0/3)	32.1
	AILGWGVK	1	1/6 - (0/3)	31.7
	LGMNFETAR	1	1/6 - (0/3)	61.7
	TYEAEKVPTGEELSK	5	5/6 - (0/3)	78.4
	DSVVLCQNAGVK	1	1/6 - (0/3)	52.2
	MVTGDNVQTAR	4	3/6 - (0/3)	91.3
	FIPVPAAPISNK	2	2/6 - (0/3)	39.3
ACA10				
	DQNIGALQELGGVR	5	5/6 - (0/3)	108.9
	GIHGDDDDILK	3	3/6 - (0/3)	55.7
	SAFGSNTYPQKK	3	3/6 - (0/3)	42.3
	LPSAFTSILVEGIAHNTTGSVFR	1	1/6 - (0/3)	46.7
	SESGEIQVSGSPTER	6	6/6 - (0/3)	68.2
	MVTGDNIQTAK	7	6/6 - (0/3)	62.2
	AIALECGILASDSDASEPNLIEGK	1	1/6 - (0/3)	77.1
	SSPNDKLLLVQSLK	2	2/6 - (0/3)	71
	VKNTVIFNAFVICQVFNEFNAR	1	1/6 - (0/3)	52.8
	KPDEINIFR	1	1/6 - (0/3)	44.6
	LIPVPETPVSQYFR	2	2/6 - (0/3)	57.1

Figure S2. Identification of ACA8 and ACA10 peptides by mass-spectrometry analysis of immuno-purified FLS2-GFP. 21 *in vitro* grown seedlings were used either untreated or treated with flg22. Sample preparations, immuno-purifications and MS/MS analysis were performed essentially as described in Roux et al. (2011). Briefly, immuno-purifications of GFP-tagged proteins were done using the magnetic GFP-trap system from Miltenyi Biotech using an IGEPAL-solubilised protein extract (4 mg protein per mL). Beads were washed with 0.1% IGEPAL extraction buffer prior to elution in boiling Laemli buffer. **A.** Peptide coverage of ACA8 and ACA10 proteins identified in an FLS2-GFP immuno-purified complex. Peptides found in untreated samples are highlighted in green, peptides found in flg22-elicited samples are in orange, peptides found in both conditions are indicated in blue, peptides found in all biological replicates of untreated and treated samples are shown in bold. **B.** Tryptic peptides identified by HPLC-electrospray ionization-MS/MS analysis. Peptides occurring in all biological replicates are marked in bold. Reproducibility ([a]) of specific tryptic peptides out of three biological replicates of untreated or flg22-treated samples prepared from Arabidopsis plants expressing FLS2-GFP. In brackets, no peptides were detected in technical controls using wild-type plants (n=2) or plants expressing a plasma membrane addressed GFP (Lti6b-GFP; n=1).

Supplementary figure 3.

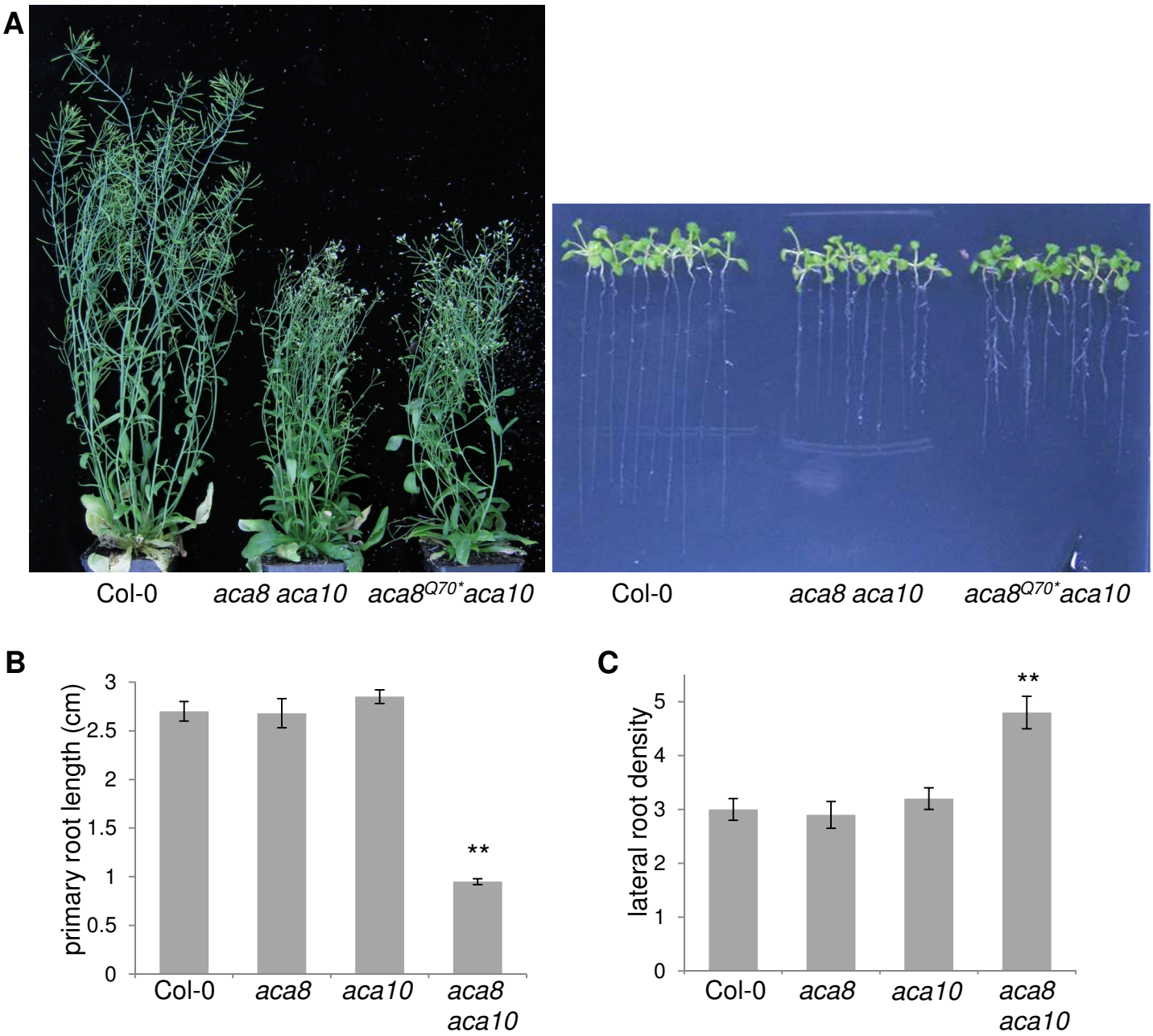

Figure S3. Developmental phenotypes of aca mutant plants. **A**. Photographs present inflorescence height and root growth of the indicated genotypes including the tilling allele aca8Q70*. **B**. Measurement of primary root growth of 8 days old seedlings, and **C**. number of lateral roots per cm primary root of 14 days old in vitro-grown seedlings of the indicated genotypes. Error bars indicate standard error based on n = 25 samples, asterisks indicate significant differences at $p<0.01$ based on T-test. **D**. Detailed view on the stem cell area of Col-0 wild type and aca8 aca10 mutant root apical meristems, 3 days after germination. Starch granules in columella cells are visible as pink dots. Note the presence of starch granules in columella stem cells in the aca8 aca10 meristem (arrow) as sign of perturbation of stem cell identity. For root phenotypic analysis, starch granules in the columella root cap were visualized with 1% Lugol solution (MERC, Germany). Seedlings were stained for 3 min, rinsed with water, cleared with chloral hydrate and analyzed using differential interference contrast optics on a Olympus BX53 light microscope and imaged using a Nikon DS-Fi1 digital camera (Lee et al., 2007).

Supplementary figure 4.

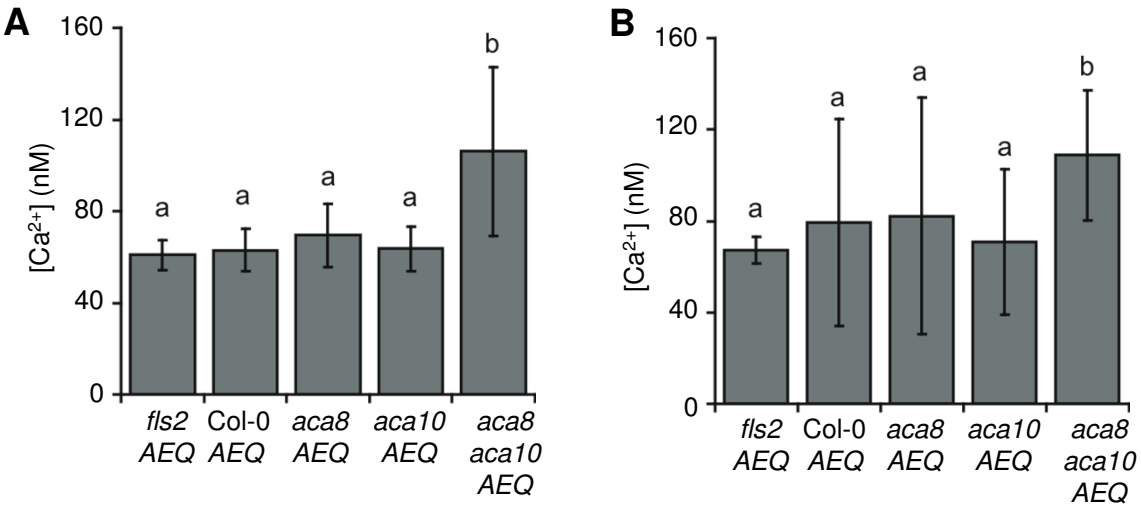

Figure S4. A. Steady-state Ca^{2+} levels before flg22-triggered Ca^{2+} burst and **B.** after the burst. Data were calculated from the absolute cytosolic [Ca^{2+}] before and at 38 min after elicitation and were averaged over two independent biological replicates. Error bars indicate standard deviations based on n = 14-16 samples, letters indicate significant differences at $p<0.05$ based on ANOVA Tukey-HSD test. Similar results were obtained at least in two independent experiments.

Supplementary figure 5.

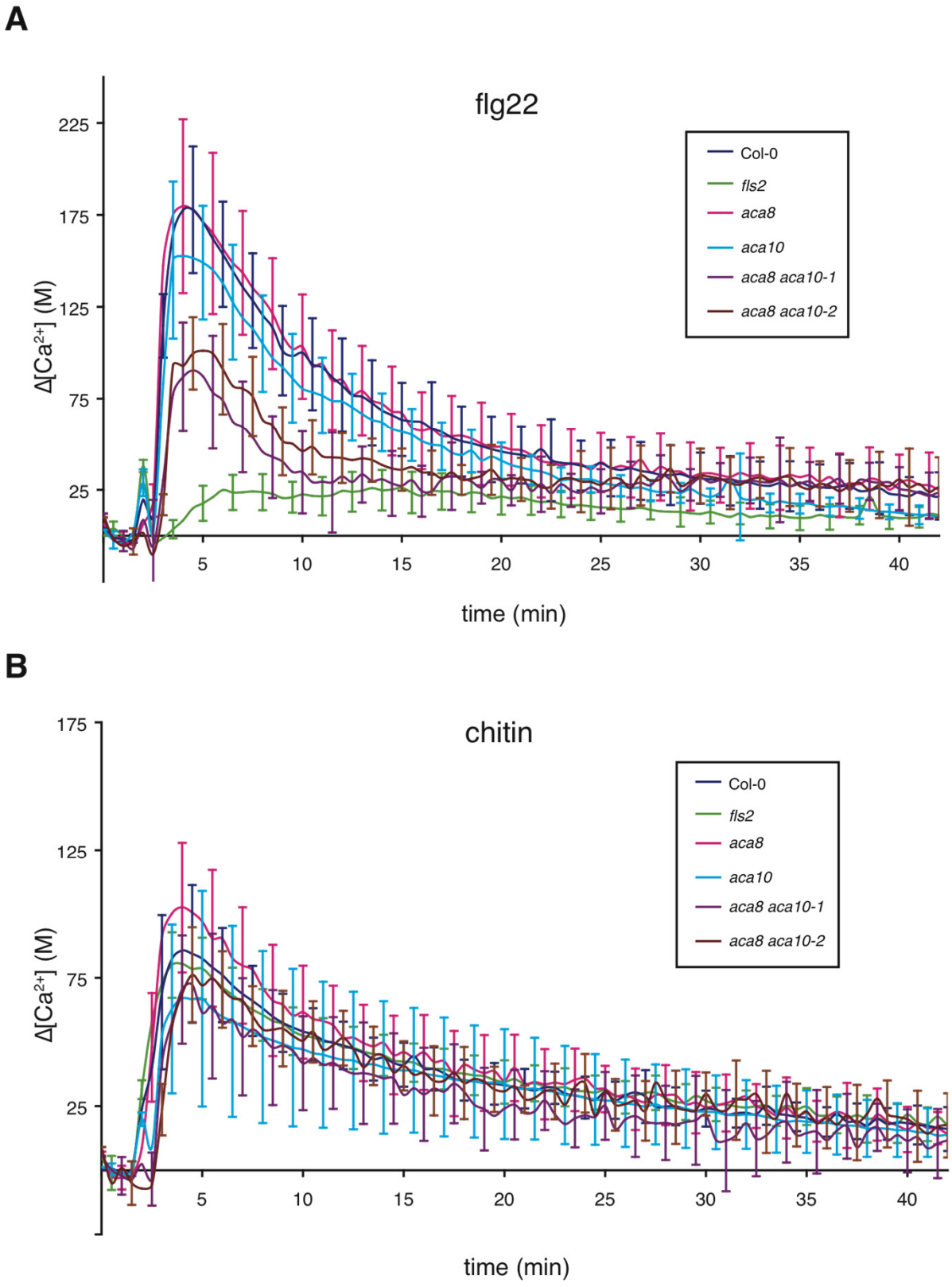

Figure S5. Patterns of the Ca^{2+} burst induced by flg22 (**A**) and chitin (**B**) over time. Included are two *aca8 aca10* lines from independent crosses showing similar results. Curves normalized to steady state cytosolic [Ca^{2+}] show Δ[Ca^{2+}] after MAMP-treatments of one representative biological experiment. Error bars show standard deviations based on n = 6-8 samples. Similar results were obtained at least in two independent experiments.

Supplementary figure 6.

A

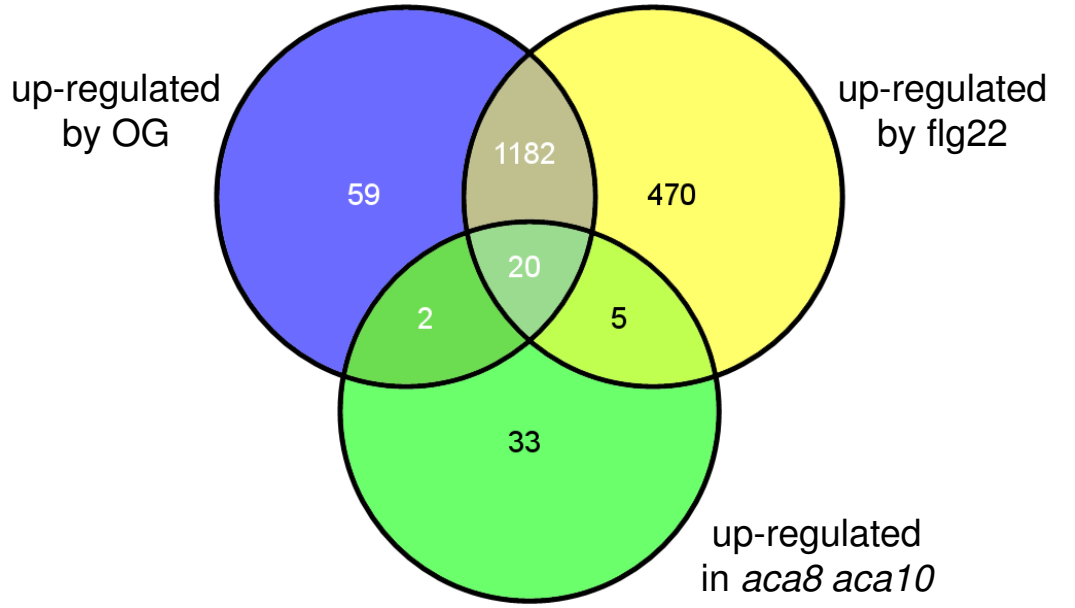

B

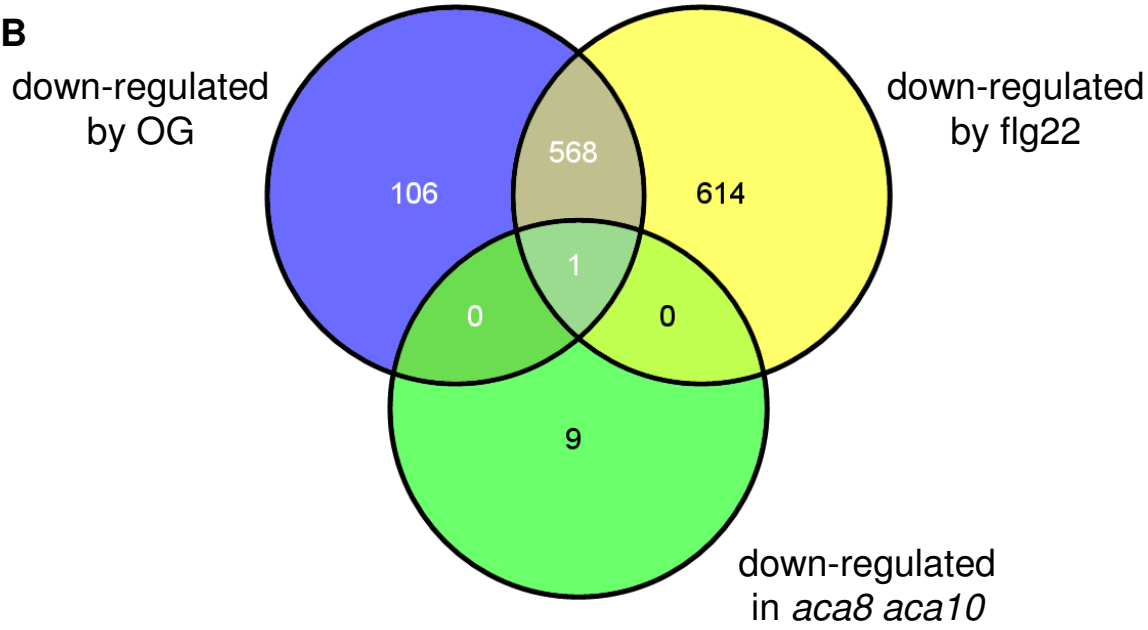

C

Gene	CPK5 log2	CPK11 log2
aca8 aca10 up-regulated genes		
At1g26380	2.6	1.9
At2g30750	1.7	1.7
At3g55470	1.1	1.1
At1g26390	1.5	2.0
At1g67980	2.5	1.5
At2g43000	1.9	1.7
At5g38900	1.2	1.0
At3g26470	nd	-1.6
At3g50770	nd	-1.6
aca8 aca10 down-regulated genes		
At1g58340	1.7	2.1
At1g55020	1.4	nd

Figure S6. Altered gene expression in *aca8 aca10* mutants. Overlap of genes up-regulated (A) and down-regulated (B) in *aca8 aca10* and upon elicitation with flg22 and oligogalacturonides (OG). Genes represented show at least two-fold regulation ($p<0.05$) within 1 hr after MPMP treatment according to Denoux et al. (2008). Nine *aca8 aca10* de-regulated genes were removed from the analysis because they were not present in the Denoux et al. (2008) study. The tool used for the Venn diagrams is available at "Venny" http://bioinfogp.cnb.csic.es/tools/venny/index.html. **C.** Flg22-induced CPK5- and CPK11-dependent expression of *aca8 aca10* de-regulated genes (asterisks) according to Boudsocq et al. (2010).

Supplementary figure 7.

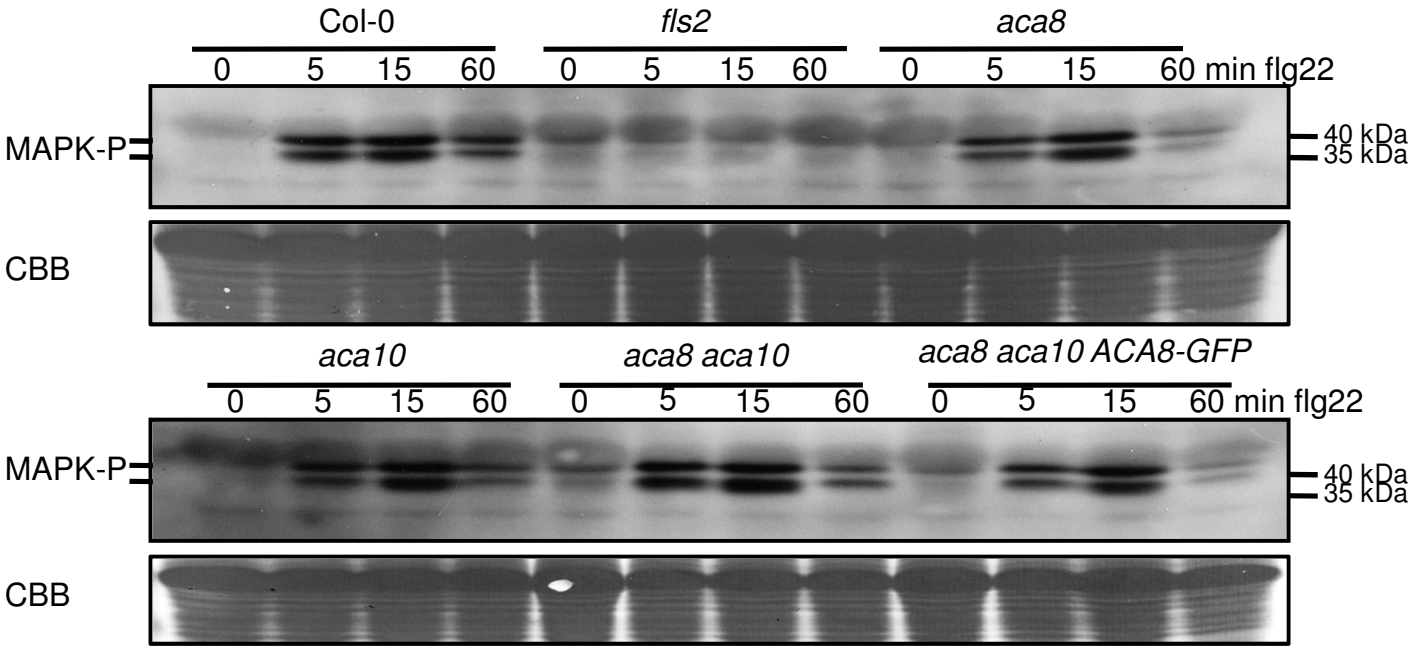

Figure S7. Protein kinase activation in flg22 signalling. MAPK activation upon flg22 application over time. Coomassie staining (CBB) is included as loading control. Similar results were obtained in at least two independent experiments.

Supplementary figure 8.

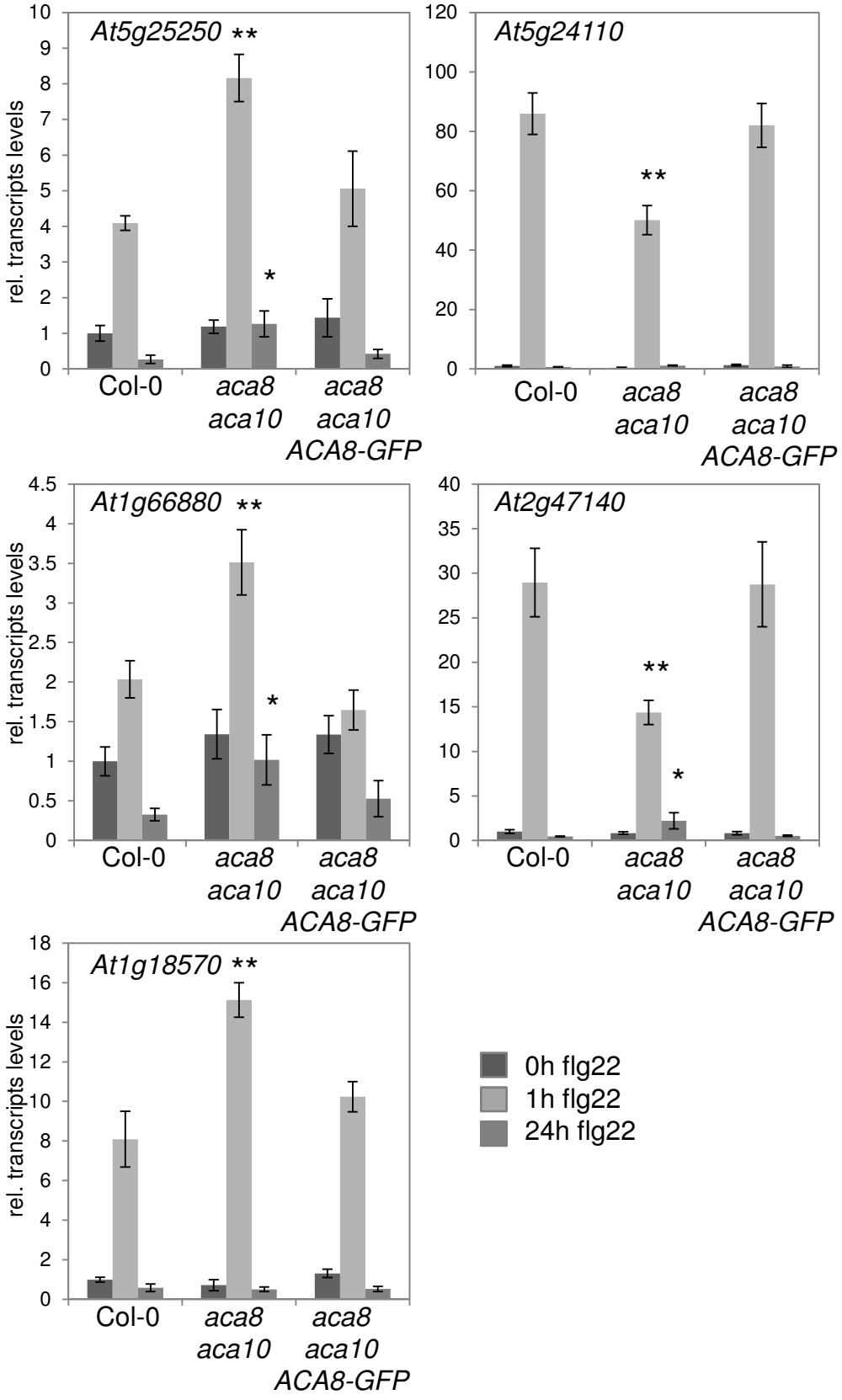

Figure S8. Expression analysis of defence marker genes. Quantitative real-time PCR monitoring transcript levels of the indicated genes in Col-0, *aca8 aca10* and *aca8 aca10 ACA8-GFP* plants. Genes in this analysis were not included by Boudsocq et al. (2010). Actin was used as control. Error bars indicate standard deviations based on n = 3 biological experiments with each three technical replicates; asterisks indicate significant differences between Col-0 and *aca8 aca10* at $p<0.05$ (*) and $p<0.01$ (**) based on Student´s T-test.